Chapter 4

NMR Spectroscopy Investigations into the DNA-Binding Properties of Dinuclear Ruthenium Complexes

4.1 INTRODUCTION

4.1.1 NMR as a Tool for Studying Nucleic Acids

Amongst the many techniques available, nuclear magnetic resonance (NMR) spectroscopy is perhaps the most powerful tool by which to characterise the structure and dynamics of oligonucleotide-small molecule interactions in solution. Traditional one-dimensional NMR techniques (typically ^{1}H, but often complimented by ^{31}P, ^{13}C and ^{15}N spectra) coupled with more elaborate two-dimensional experiments, particularly Nuclear Overhauser Effect Spectroscopy (NOESY), allows for the complete sequential and conformational assignment of oligonucleotides, as well as a means to monitor and interpret the signals of a DNA-substrate during binding events.

While preliminary NMR-based investigations into nucleic acid structure took place as early as the late 1960s,[1-4] real progress in the field came as the result of advances in two-dimensional NMR techniques in the early 1980s.[5-12] To date, structure-assignment by means of NMR data has been employed across a range of different nucleic acid sequences and conformations, including molecules which incorporate such non-canonical features as bulges and hairpin loops.[13-21] Measurement of proton-proton coupling constants provides invaluable data regarding sugar puckers and glycosidic bond angles, and NOE data from two-dimensional experiments provide an indication of through-space proton-proton distances and facilitates the sequential assignment of adjacent bases. In addition, base-pairing may be observed through the presence of imino proton resonances. The sum total of all such data provides a reliable means to assess the overall conformation of a given oligonucleotide, but certain aspects (such as groove dimensions) may only be indirectly derived from such observations. Solution-phase NMR structures are of greater physiological relevance than solid-state crystal structures, with the former technique highlighting the inherent flexibility of DNA and the dynamic motion of its constituent residues. Nevertheless, the structural data obtained through NMR experiments is generally of a lower effective ‘resolution’ than that obtained by crystallographic analyses, owing to the relatively small amount of NOE data available and lack of long-range NOEs; accordingly, the two techniques are often considered to be complementary in conformational studies of nucleic acids.[22]

NMR experiments also provide valuable data regarding the dynamics and locality of small molecule-DNA interactions. The binding kinetics of such associations may be inferred from the

resultant broadening of resonances in one-dimensional spectra, while the observation of intermolecular NOE signals between the oligonucleotide and its substrate can be used to determine the specific binding site and orientation of the latter. Such experiments have been widely employed in the study of non-covalent interactions involving molecules such as antibiotics,[23-30] dyes,[31-33] proteins,[34-38] and metal complexes,[39-41] as well as the formation of adducts between oligonucleotides and small covalently-binding molecules.[42-48] Given the practical difficulties involved in obtaining crystals of metal complex-nucleic acid associations and the greater relevance of solution-based measurements, NMR is the foremost tool by which the structural basis of such interactions can be characterised. Thus, NMR experiments have been frequently used to study the nucleic acid-binding properties of mononuclear intercalating polypyridylruthenium(II) complexes,[49-53] including the contentious binding scenarios of $[Ru(phen)_3]^{2+}$ [54-57] and $[Ru(phen)_2(dppz)]^{2+}$.[58, 59]

4.1.2 NMR Investigations of Groove-Binding Dinuclear Species

In recent years, collaborations between the laboratories of F. R. Keene (James Cook University) and J. G. Collins (University of New South Wales, Australian Defence Force Academy) have sought to explore the oligonucleotide interactions of *dinuclear* polypyridylruthenium(II) complexes, with NMR experiments (^{1}H, DQFCOSY and NOESY) serving as the foundation of these investigations. The earliest of these studies dealt with the three stereoisomers of the non-intercalating complex $[\{Ru(Me_2bpy)_2\}_2(\mu\text{-bpm})]^{4+}$ and their interactions with two duplex oligonucleotides, $d(CAATCCGGATTG)_2$ and $d(CAATCGCGATTG)_2$.[60, 61] The observation of NOEs between the metal complex and H1′/H4′ sugar protons established the minor groove as the preferred binding site of the dinuclear complex, despite its inherent bulk. These NOEs were strongest in the case of the ΔΔ enantiomer; this evidence, coupled with the observation of significant changes in the chemical shifts of ΔΔ-$[\{Ru(Me_2bpy)_2\}_2(\mu\text{-bpm})]^{4+}$ resonances upon binding, suggest that this stereoisomer underwent the strongest association. By contrast, the spectrum of the ΛΛ enantiomer remained relatively unperturbed and the *meso* form exhibited two sets of resonances, each reminiscent of that belonging to one of the bound enantiomers. Interestingly, the locality of NOE cross-peaks in the NOESY spectra implied that ΔΔ-$[\{Ru(Me_2bpy)_2\}_2(\mu\text{-bpm})]^{4+}$ bound preferentially to the central CC/GG region (and, to a lesser extent, the termini)

of d(CAATCCGGATTG)$_2$, but with d(CAATCGCGATTG)$_2$ the AAT/ATT sequence was the more favourable (again, along with the termini). This primary preference for the CC/GG site in d(CAATCCGGATTG)$_2$ is attributed to the more open, hence more accommodating, minor groove at this site relative to the adjacent AT-rich sites. Conversely, the introduction of the alternating CGCG sequence in the dodecanucleotide d(CAATCGCGATTG)$_2$ is likely to have resulted in steric clashes between the metal complex and minor groove guanine amino groups, thus forcing the complex into the minor groove of the adjacent AT-rich sites. Relatively weak binding constants of 3×10^3 and 1×10^4 M^{-1} were calculated for ΔΔ-[{Ru(Me$_2$bpy)$_2$}$_2$(μ-bpm)]$^{4+}$ binding to d(CAATCCGGATTG)$_2$ and d(CAATCGCGATTG)$_2$, respectively. Analogous experiments with the enantiomers of [{Ru(bpy)$_2$}$_2$(μ-bpm)]$^{4+}$ revealed slightly larger binding affinites, most likely arising from a better fit to the narrow minor groove in the absence of bulky methyl groups, and a preference for AT-rich sites on the duplex.[61]

Given this relatively weak association between the dinuclear complex and duplex DNA and the indication of a preference for larger spatial regions, it was decided to investigate more spatially-accommodating targets. Prior studies into the DNA-binding ability of HAT-bridged dinuclear species revealed a preference for partially-denatured DNA over the confined grooves of the double-helical duplex.[62-64] Thus, an oligonucleotide featuring a non-duplex structural aberration was selected as a potential target for [{Ru(Me$_2$bpy)$_2$}$_2$(μ-bpm)]$^{4+}$, specifically a tridecanucleotide possessing an unpaired adenine base (or "bulge") {d(CCG**A**GAATTCCGG)$_2$}. It was proposed that the more open and/or flexible bulge site would serve as an ideal binding site for the metal complex, and this was indeed observed in studies that contributed towards the present author's Honours Thesis.[65-67] One- and two-dimensional NMR experiments revealed total enantioselectivity in the binding of [{Ru(Me$_2$bpy)$_2$}$_2$(μ-bpm)]$^{4+}$ to the bulge site: addition of the ΔΔ enantiomer induced significant broadening and shifting of metal complex resonances, notable shifts in bulge-site proton resonances, and the observation of several strong NOE signals to the minor groove of base residues at or around the bulge site. A binding constant of $\geq 10^5$ M^{-1} was determined by monitoring the change in metal complex resonance chemical shifts during the titration process. Conversely, only minor chemical shift changes were seen upon the addition of the ΛΛ enantiomer, with only weak NOEs to the frayed termini of the tridecanucleotide observed in NOESY spectra. The *meso* diastereoisomer once again yielded two sets of metal complex resonances upon binding; a small number of strong NOEs were noted to the bulge site in

addition to a range of less intense cross peaks to a variety of minor groove proton resonances over the length of the oligonucleotide. A binding constant of 4×10^4 M^{-1} was determined for this isomer. Overall, these results were indicative of strong, selective binding to the bulge site by the ΔΔ enantiomer, relatively weak binding to the ends of the duplex by the ΛΛ enantiomer, and binding of intermediate strength and selectivity by the *meso* diastereoisomer. The selectivities of the enantiomers were confirmed through competitive binding titrations.

In accompanying experiments, ΔΔ-$[\{Ru(Me_2bpy)_2\}_2(\mu\text{-bpm})]^{4+}$ was found to bind comparatively weakly (4×10^3 M^{-1}) to a non-bulged control sequence, $d(CCGGAATTCCGG)_2$, and non-selectively (NOEs were observed to the termini and the central AATT region), confirming the enhanced affinity of this class of metal complex for more open, non-duplex nucleic acid structures. Additionally, the analogous metal complexes with mixed methylated and non-methylated bipyridine terminal ligands, ΔΔ-$[\{Ru(Me_2bpy)_2\}(\mu\text{-bpm})\{Ru(bpy)_2\}]^{4+}$, and only non-methylated bipyridine terminal ligands, ΔΔ-$[\{Ru(bpy)_2\}_2(\mu\text{-bpm})]^{4+}$, were titrated with the bulge sequence in order to investigate the potentially important role of the methyl groups.[65, 68] The mixed-terminal ligand complex was found to bind to the bulge sequence with an affinity and selectivity similar to that of ΔΔ-$[\{Ru(Me_2bpy)_2\}_2(\mu\text{-bpm})]^{4+}$ (i.e. it bound to the bulge site with $K_a \geq 10^5$ M^{-1}), while ΔΔ-$[\{Ru(bpy)_2\}_2(\mu\text{-bpm})]^{4+}$ is believed to bind somewhat less strongly. Intriguingly, the observed broadening and upfield shifts of resonances in ΔΔ-$[\{Ru(Me_2bpy)_2\}(\mu\text{-bpm})\{Ru(bpy)_2\}]^{4+}$ were all more pronounced for those resonances corresponding to the Me_2bpy ligand protons. Furthermore, the strongest and most abundant NOE signals seen in NOESY spectra were between bulge site oligonucleotide protons and those same Me_2bpy protons. Molecular modelling based on the available NOE data suggested that the binding orientation of ΔΔ-$[\{Ru(Me_2bpy)_2\}(\mu\text{-bpm})\{Ru(bpy)_2\}]^{4+}$ was such that the Me_2bpy ligands (and associated metal centre) were projected into the minor groove at the bulge site while the end with the non-methylated ligands jutted out from the groove to some extent. This binding model, coupled with the lower apparent affinity of ΔΔ-$[\{Ru(bpy)_2\}_2(\mu\text{-bpm})]^{4+}$ for the bulge sequence, is indicative of a significant binding contribution by the methyl groups, most likely due to van der Waals or hydrophobic interactions with the accommodating bulge site. The contribution of methyl substituents is well-known in the nucleic acid-binding of polypyridylruthenium(II) complexes.[69, 70]

Recently, in experiments conducted by Dr. Caitriona Spillane and involving the present author, the nucleic acid-binding of ΔΔ- and ΛΛ-$[\{Ru(Me_2bpy)_2\}_2(\mu\text{-bpm})]^{4+}$ has been further

explored in the context of RNA; specifically, the interactions of these metal complexes with the oligonucleotides r(CCG**A**GAAUUCCGG)$_2$ and r(CCGGAAUUCCGG)$_2$ (which are RNA analogues of the bulge and non-bulged control DNA sequences used in the above studies).[71] The minor groove of A-form RNA is significantly different from that of its B-form DNA counterpart and thus might be conceived as a potentially less inviting target to the bulky dinuclear ruthenium complexes. However, the associations between [{Ru(Me$_2$bpy)$_2$}$_2$(μ-bpm)]$^{4+}$ and RNA proved to be very reminiscent of the same interactions with DNA. As with the DNA-based NMR experiments, both enantiomers bound to the bulge-free control sequences quite weakly; upon the binding of the ΔΔ enantiomer upfield shifts of metal complex resonances inferred an association constant of 1×10^3 M^{-1}, with NOE data indicating that the frayed termini of the RNA duplex were the preferred binding location. Binding of the ΛΛ enantiomer induced negligible changes to metal complex or dodecanucleotide resonances. ΔΔ-[{Ru(Me$_2$bpy)$_2$}$_2$(μ-bpm)]$^{4+}$ was found to bind to the bulge-containing RNA with a significantly higher affinity (6×10^4 M^{-1}) than the control sequence. Selective changes in the chemical shifts of resonances pertaining to minor groove protons in the vicinity of the bulge site, and the observation of a number of significant intermolecular NOEs to the bulge site from the metal complex, were indicative of selective binding by the complex to the bulge site. The results of competitive binding experiments suggest that the ΛΛ enantiomer binds to bulge RNA tridecanucleotide with a similar affinity to the ΔΔ enantiomer. Thus, while the selectivity of the metal complex for more open nucleic structures (i.e. the bulge site) remains evident even under significantly altered groove dimensions, the observed enantioselectivity of [{Ru(Me$_2$bpy)$_2$}$_2$(μ-bpm)]$^{4+}$ seems to be negated when binding to A-form RNA.

Alternations in the identity of the terminal ligands have also been investigated with respect to its affect on the affinity and selectivity of nucleic acid-metal complex interactions. Inspired by the affinity and enantioselectivity of [{Ru(Me$_2$bpy)$_2$}$_2$(μ-bpm)]$^{4+}$ and fluorescent intercalator displacement (FID) assay results implying a greater affinity by complexes with phen or Me$_2$phen terminal ligands (refer to Chapter 3 for further details), NMR techniques were used to study the binding of [{Ru(phen)$_2$}$_2$(μ-bpm)]$^{4+}$ to the bulge-containing DNA tridecanucleotide d(CCG**A**GAAATTCCGG)$_2$.[72] It is noteworthy that FID results implicate the *meso* isomer as the strongest binding of the three stereoisomers. This observation correlates with NMR results which found that the *meso* isomer produces less structural perturbation to the minor groove upon binding than do either of the enantiomers; for all three stereoisomers, it was the

resonances of minor groove protons corresponding to residues at or around the bulge site that underwent the most significant changes in chemical shift. All metal complex resonances underwent significant broadening upon binding suggesting relatively strong binding, and the *meso* diastereoisomer once again exhibited two sets of resonances (one set being relatively unchanged from the chemical shifts of the free complex, the other having undergone significant upfield shifts). NOE data for all three complexes situate their preferential binding regions at the bulge site of the tridecanucleotide, albeit with greater specificity and a position somewhat further towards the centre of the duplex in the case of the *meso* diastereoisomer. Furthermore, the NOEs between the ΔΔ and ΛΛ enantiomers and the bulge site were significantly weaker than those exhibited to the *meso* form. These observations, in conjunction with molecular modelling experiments, imply selective binding at the bulge site by all three stereoisomers, albeit with greater affinity in the case of the *meso* diastereoisomer due to more favourable steric interactions.

The affinity for the bulge-containing DNA sequence d(CCG**A**GAATTCCGG)$_2$ by the flexible ligand-bridged metal complex ΔΔ-[{Ru(phen)$_2$}$_2$(μ-bb7)]$^{4+}$ was also examined. Modified fluorescent dye-displacement assays revealed that, for a series of metal complexes having bridging ligands that differ only in the length of their flexible methylene linkers, the bb7-bridged species (specifically the ΔΔ enantiomer) with its heptane linker bound the strongest to the bulge tridecanucleotide.[73] NMR investigations showed that the favourable binding of the metal complex may be due to an optimal linkage length which allows one metal centre to bind strongly at the bulge site while the other associates favourably but more loosely with the AT-rich region at the centre of the duplex. Resonances from the metal complex were universally broad upon binding, whereas some selective broadening of the bulge-site and AATT minor groove resonances was observed in the oligonucleotide spectrum at low metal complex-to-oligonucleotide ratios. NOEs were abundant but difficult to assign due to the broadening of oligonucleotide resonances; nevertheless, a number of intermolecular cross peaks between the complex and the minor groove of the bulge site could be identified along with a number of less intense signals to the central AATT region. Molecular modelling experiments based upon the available NMR data placed one metal centre in the minor groove at the bulge site orientated such that a phen ligand might be poised for partial intercalation, while the other metal centre assumed a less snug association with the central AATT region. The hydrocarbon linker between the two metal centres was secreted away in the minor groove. Such a model

implies that one can conceivably "fine-tune" the binding properties of flexibly-bridged species by carefully selecting linker lengths that reflect the separation between two favourable binding sites on an oligonucleotide (two different bulge sites, for instance).

A number of larger bulge sites were also investigated in the FID assay, with dppm-bridged metal complexes appearing to bind particularly well to the larger non-duplex site. Specifically, ΔΔ-[{Ru(phen)$_2$}$_2$(μ-dppm)]$^{4+}$ demonstrated a high affinity for the triple adenine bulge in the oligonucleotide d(GCATCG**AAA**GCTACG)•d(CGTAGCCGATGC).[74] Selective broadening of bulge site minor groove proton resonances and the confinement of all notable NOEs to this section of the spectrum confirmed the bulge site as the preferred binding location. NMR titrations allowed for the determination of a binding constant – 4×10^5 M^{-1}. Molecular modelling was once again used to elucidate upon the binding of the metal complex, with the smaller helical twist of the oligonucleotide at the AAA bulge complementing the obtuse angle of the dppm bridge as it follows the minor groove.

4.1.3 Present Studies

Each of the NMR investigations detailed above highlights the preference of bulky dinuclear polypyridylruthenium(II) complexes for more open structures in the minor groove of oligonucleotides. Furthermore, variations to both the terminal and bridging ligands can significantly alter the specific preferences of the metal complexes. As described in the previous Chapter, FID assays revealed that as a general rule metal complexes with phen-based terminal ligands typically underwent stronger associations than did those with bpy-based ligands. Also, the addition of methyl substituents to the terminal ligands was found to further increase the affinity of these complexes for nucleic acids. With regards to bridging ligands, it was found that bpm-bridged species demonstrated a greater selectivity for bulge sites, whereas metal complexes based on the angular bridging ligands such as HAT demonstrated a particular affinity for hairpin loop-containing oligonucleotides.

In order to elucidate the apparent hairpin selectivity of HAT-bridged complexes, a series of NMR experiments (involving both one- and two-dimensional techniques) were undertaken with several different oligonucleotides. Described below are some preliminary investigations – essentially negative controls – into the relatively poor association between the standard bulge tridecanucleotide d(CCG**A**GAATTCCGG)$_2$ {and its control sequence, d(CCGGAATTCCG)$_2$}

and the HAT-bridged complexes $[\{Ru(Me_2bpy)_2\}_2(\mu\text{-HAT})]^{4+}$ and $[\{Ru(bpy)_2\}_2(\mu\text{-HAT})]^{4+}$. The association between $[\{Ru(bpy)_2\}_2(\mu\text{-HAT})]^{4+}$ and an oligonucleotide featuring a 4-base hairpin loop, {d(CACTGGT**CTCT**ACCAGTG)}, is also investigated. The crux of these NMR studies is the strong association between the complexes $[\{Ru(Me_2phen)_2\}_2(\mu\text{-HAT})]^{4+}$ and $[\{Ru(phen)_2\}_2(\mu\text{-HAT})]^{4+}$ and a 6-base hairpin loop, d(CACTGGT**CTCTCT**ACCAGTG), which were found to induce significant fluorescence decreases in FID assays.

The remaining NMR experiments described in this Chapter deal with a somewhat different scenario – the binding of $[\{Ru(phen)_2\}_2(\mu\text{-ppz})]^{4+}$ to a *duplex* oligonucleotide, specifically $[d(AT)_6]_2$. This system is quite unusual in that, as previously mentioned, bulky dinuclear complexes generally prefer to bind to more open and/or flexible deformations to the canonical DNA double-helix, whereas FID assay results suggest that $[\{Ru(phen)_2\}_2(\mu\text{-ppz})]^{4+}$ has an affinity for this specific duplex sequence that is equal-to or greater than its affinity for any bulge or hairpin sequence. While the favourable electrostatics of AT-rich sequences is known to be attractive to cationic metal complexes, one would expect the confines of the minor groove $[d(AT)_6]_2$ to be such that the dinuclear species would associate comparatively poorly. Thus, this association presents an intriguing target for not only NMR experiments, but an accompanying restriction enzyme inhibition assay.

The binding of $[\{Ru(phen)_2\}_2(\mu\text{-ppz})]^{4+}$ to the narrow minor groove of an AT sequence suggests some parallels to the TATA-binding protein (TBP) which plays an important role in eukaryotic transcription.[75, 76] TBP is unusual amongst DNA-binding proteins in that it binds to the *minor* groove rather than the information-rich major groove.[77, 78] The protein binds to a DNA sequence known as a TATA box which, as the name suggests, is a highly-conserved consensus sequence built upon a core of alternating thymine and adenine nucleobases.[79] TATA boxes are found in the promoter region of most eukaryotic genes; upon binding, TBP melts and unwinds the double-helical AT-rich DNA and in its role as a subunit of the transcription factor TFIID, begins recruiting other necessary factors to the site so that RNA Polymerase II may begin transcription of the gene. Metal complexes which mimic the binding selectivity of TBP have potential pharmaceutical applications as they can potentially inhibit the binding of the protein, thus down-regulating transcription. The resultant cytotoxic effect would have potential anti-tumour applications.[80] In an effort to assess the inhibitive ability of $[\{Ru(phen)_2\}_2(\mu\text{-ppz})]^{4+}$, restriction enzyme inhibition assays were conducted with the restriction endonuclease *Bst*Z17I. This enzyme cleaves DNA at the middle of the sequence GTATAC (i.e. the centre of a

TATA box), thus the ability of the metal complex to interfere with the function of TBP can be inferred from its ability to restrict the cleavage activity of *Bst*Z17I.

4.2 EXPERIMENTAL

4.2.1 Materials

Oligonucleotides were obtained from GeneWorks. Acetonitrile (Merck) and methanol (HPLC grade; Ajax) were used as supplied. D_2O (both 99.9% and 99.96%) was obtained from Cambridge Isotope Laboratories while SP and CM Sephadex C-25 were obtained from GE Healthcare Biosciences (formerly Amersham Pharmacia Biosciences). All aqueous solutions intended for NMR studies were made up in doubly-distilled and de-ionised Milli-Q water. C18 Sep-Pak reverse-phase chromatographic cartridges were acquired from Waters. All metal complexes used in these studies were prepared as described in Chapter 2 and converted to water-soluble chloride salts using the technique described in Chapter 3.

The restriction endonuclease BstZ17I was obtained from New England BioLabs, ethidium bromide (HPLC grade) from Fluka, Agarose-HR from Ambion, sodium chloride (NaCl) from Ajax, glycerol from APS Finechem, and 10X TBE buffer solution from National Diagnostics.

4.2.2 Physical Measurements

400 MHz NMR spectra were recorded on a Varian Unity*plus*-400 spectrometer (University of New South Wales, Australian Defence Force Academy); 800 MHz spectra were recorded on a Bruker Avance 800 spectrometer (Australian National University). Oligonucleotide concentrations were determined from UV absorbances at 260 nm using either a Cary 50 Bio UV/Vis or a Cary 5E UV/Vis/NIR spectrophotometer.

4.2.3 NMR Procedures

^{1}H NMR experiments were performed at either 400 or 800 MHz. The discussion below refers to the results of 400 MHz experiments unless specifically noted otherwise. Phase-sensitive NOESY spectra were acquired using the method of States *et al.*,[81] with 2048 data points in t_2 for 256 t_1 values with a pulse repetition delay of 1.7 s. Mixing times ranged from

100 to 350 ms. DQFCOSY spectra were obtained using a similar data set. Two-dimensional NMR data sets were zero-filled to 1024 points in the t_1 dimension and apodised with either a Gaussian or shifted sinebell function. Spectra were recorded at 25 °C in 99.96% D_2O unless otherwise noted.

4.2.3.1 Oligonucleotide Preparation

Oligonucleotides were prepared using a reverse-phase Waters C18 Sep-Pak cartridge. The cartridge was activated with methanol (10 mL) and water (2 × 10 mL) prior to loading an aqueous solution of the oligonucleotide being prepared. The Sep-Pak was then washed with water (2 × 3 mL) and the oligonucleotide subsequently eluted under gravity with a 50% v/v acetonitrile/water solution. Several fractions of approximately 2 mL each were collected and those containing the oligonucleotide (as determined spectrophotometrically) were freeze-dried.

Once purified, the oligonucleotides were converted from the supplied triethylammonium salts to sodium salts by means of cation-exchange chromatography on a CM Sephadex C-25 column pre-equilibrated with 1 M NaCl. The lyophilised oligonucleotides were loaded on the column in aqueous solution and eluted with water. Again, several fractions were collected and those found to have the largest absorbance at 260 nm were combined together with 650 μL of phosphate buffer (10 mM, pH 7.0) containing 20 mM NaCl and 1 mM Na_2H_2EDTA then freeze-dried. The oligonucleotides were subsequently re-lyophilised several times from D_2O (99.9%) in order to replace exchangeable protons. Finally, the freeze-dried oligonucleotide/buffer mixtures were dissolved in 99.96% D_2O (650 μL) for use in NMR analyses. Oligonucleotide concentrations {typically 0.8 to 1.5 mM (duplex concentration)} were determined spectrophotometrically using an ε_{260} value of 6,600 M^{-1} cm^{-1} (nucleotide concentration).[82]

4.2.3.2 NMR Titrations

Stock solutions of the metal complexes (chloride salts; 15-20 mM) to be used in NMR titrations were prepared in 99.96% D_2O and additions made directly into the NMR tube containing the oligonucleotide sample being investigated. One-dimensional proton spectra were

typically obtained at metal complex-to-oligonucleotide equivalents of 0.1, 0.2, 0.4, 0.6, 0.8, 1.0 and 2.0, while NOESY and DQFCOSY were generally recorded at 1:1 or 2:1 ratios.

4.2.3.3 Determination of Binding Constants

The metal complex-DNA associations being investigated may be represented by the equation M + DNA ⇌ M—DNA, where M is the free metal complex, DNA is the free oligonucleotide, and M—DNA is the metal complex-bound oligonucleotide. The association constant for this interaction may be expressed as:

$$K_{ass} = \frac{[\mathrm{M-DNA}]}{[\mathrm{M}][\mathrm{DNA}]} \qquad \textbf{(Equation 4.1)}$$

The concentrations to be used in Equation 4.1 may be estimated from the known original concentrations of the metal complex and oligonucleotide, with the relative concentrations of free and bound metal complex derived using the equation described by Eriksson *et al.*,[56]

$$\delta_o = \chi_f \delta_f + \chi_b \delta_b \qquad \textbf{(Equation 4.2)}$$

where δ_o is the observed chemical shift of the metal complex resonances, χ_f and χ_b are the mole fractions of the free and bound metal complex, respectively, and δ_f and δ_b are the chemical shifts of the resonances of the free and bound metal complexes. Under appropriate circumstances, the δ_b value can be determined from the shift at the lowest ratio of metal complex to oligonucleotide for which the resonance can be assigned, while the value for δ_f is taken from the spectrum of the free metal complex in an identical buffer solution.

4.2.4 Molecular Modelling

Molecular modelling experiments were conducted using the software packages HyperChem 7.5[83] and MS Modeling 3.2.[84] Oligonucleotide models were constructed using the nucleic acid-building functionality of the HyperChem program: duplex nucleotides were input as standard B-DNA type base pairs while bulges and loops, where applicable, were entered as single-

stranded residues. Phosphate backbone angles between single-stranded residues and duplex portions of the oligonucleotides were manipulated to ensure all covalent links were within acceptable limits. The oligonucleotide models were further refined using observed NOE data to approximate the solution structure as closely as possible. The AMBER99 molecular mechanics force field set, having been extensively modified to reflect the observed behaviour of biological macromolecules such as DNA,[85] was used to ultimately optimise the oligonucleotide model.

Metal complex models were constructed using either the HyperChem or MS Modeling interfaces and subsequently geometry optimised using the ZINDO/1 or Forcite/Universal Force Field methods, respectively. ZINDO/1 is a semi-empirical quantum mechanics method of calculating molecular orbitals that was designed for the treatment of transition elements,[86] while the UFF employed by the Forcite molecular mechanics package has also seen extensive successful application to the modelling of metal complexes.[87, 88]

The metal complex model was then manually docked at the approximate site on the oligonucleotide as suggested by available NMR data and the system then optimised using AMBER99 (HyperChem) or the Consistent Valence Force Field (CVFF)[89] functionality of the Discover molecular simulation module (MS Modeling). Energy-distance restraints were applied to ensure specific observed non-bonded interactions between the metal complex and the oligonucleotide were maintained. The final optimisation was applied only to the oligonucleotide conformation, with the geometry and charge distribution of the complex held rigid. Due to the number of atoms within the system, computational limitations necessitated the implicit treatment of solvent molecules. Optimisation procedures were conducted *in vacuo* using the available force field and a Polak-Ribiere conjugate-gradient algorithm with a 5×10^{-5} kcal M^{-1} $Å^{-1}$ convergence criteria. In an effort to examine a range of possible binding modes, the minimisation procedure for each case was reproduced from a variety of subtly different starting orientations (compliant with available NOE constraints).

4.2.5 Restriction Endonuclease Inhibition Assay

4.2.5.1 Preparing the TATA Box Sequence Oligonucleotide

Initially, the TATA box sequence-containing oligonucleotide was constructed from its two constituent 40 nt single strands (GeneWorks): 5′-GGC ACG TGG AAC TCT GGG **TAT A**CT CAG CGA GGC CTA CTC G-3′ and 5′-CGA GTA GGC CTC GCT GAG **TAT A**CC CAG

AGT TCC ACG TGC C-3′. Each single strand was rehydrated/dissolved in a 5 mM Tris buffer solution (500 μL; pH 7.5) containing 50 mM NaCl. The concentration of each single strand was determined spectrophotometrically using extinction coefficients provided by the supplier, and appropriate volumes of each were combined to achieve a 1:1 molar ratio of the two. Annealing of the complimentary strands was accomplished by heating the mixture to 80 °C in a hot water bath before allowing it to cool slowly back to room temperature. The concentration of the TATA sequence duplex – measured using an extinction coefficient for calf thymus DNA (ε_{260} = 12,824 M^{-1} cm^{-1} bp^{-1})[90] – was adjusted to 25 μM (bp) with the aforementioned Tris buffer solution.

4.2.5.2 Digesting the Oligonucleotide

Stock solutions of the metal complex being investigated – $[\{Ru(phen)_2\}_2(\mu\text{-ppz})]Cl_4$ – were prepared in Tris buffer solution. Aliquots of the TATA oligonucleotide (20 μL) were added to individual microfuge tubes and equilibrated with small volumes of the metal complex, the final concentration of which varied from 0-200 μM. To each tube was added the reaction buffer supplied with the restriction enzyme (3 μL ; 10X "NEBuffer3", diluted to 1X concentration in the final reaction mixture: 100 mM NaCl, 50 mM Tris-HCl, 10 mM $MgCl_2$, 1 mM DTT), and 10 U (2 μL) of the restriction enzyme *Bst*Z17I itself. The tubes (30 μL total reaction volume each) were subsequently incubated in a water bath at 37 °C for four hours.

It was found that removal of the metal complex from the reaction mixture prior to loading it on a gel was desirable because the complex interfered with the visualisation of the gel by interacting with – and reducing the fluorescence of – ethidium bromide (which is not surprising considering the nature of the fluorescent intercalator displacement assay described in Chapter 3). To prevent this interference, a small amount of SP Sephadex C-25 cation-exchange (*ca.* 10 mg) was added to each of the reaction tubes after incubation in order to adsorb the cationic metal complex. Each reaction mixture was subsequently centrifuged to collect the Sephadex at the bottom of the tube, allowing the metal complex-free supernatant solution to be pipetted off and run in a gel.

4.2.5.3 Running the Gel

A 2.5% (w/v) agarose gel was prepared by adding Agarose-HR (1.5 g) to 1X TBE buffer (0.089 M Tris-borate, 2 mM Na_2EDTA; 60 mL) and heating in a microwave oven (high power, 30 second intervals) until dissolved. Once sufficiently cooled (*ca.* 50 °C), ethidium bromide solution (3 μL; 10 mg/mL) was thoroughly mixed into the solution before it was poured into a mould and allowed to set for approximately 30 minutes. Once set, the gel was submerged in 1X TBE buffer solution in an electrophoresis tank (Biorad Sub-Cell GT).

Aliquots of the digest solutions (12 μL) were combined with loading buffer {30% glycerol (v/v) in water, 3 μL} and loaded into the wells of the agarose gel. Electrophoretic separation was performed at 100 V for 60 minutes and the gels were visualised and documented using a UV light/video camera setup (Fotodyne Inc. FotoEclipse).

4.3 RESULTS & DISCUSSION

4.3.1 Assignment of Metal Complex Resonances

The assignment of free metal complex resonances were made based on one-dimensional as well as NOESY and DQFCOSY experiments recorded in D_2O (99.9%) using 1 mM solutions of the desired metal complex in the phosphate buffer solution described above, and by comparison to the CD_3CN-based spectra previously acquired (refer to Chapter 2).

4.3.2 Assignment of Oligonucleotide Resonances

The ^{1}H NMR resonances of several of the oligonucleotides used in these studies have been previously assigned: the adenine bulge-containing tridecanucleotide d(CCG**A**GAATTCCGG)$_2$ and its canonical control dodecanucleotide d(CCGGAATTCCGG)$_2$ by Kalnik *et al.*[91] and Patterson *et al.*,[65] repectively, and the four-base hairpin loop sequence d(CACTGGT**CTCT**ACCAGTG) by Henderson *et al.*[92] The analogous 6-base hairpin loop sequence d(CACTGGT**CTCTCT**ACCAGTG) and AT dodecanucleotide d(ATATATATATAT)$_2$ were assigned (where possible) using standard techniques.

Despite the superficial complexity of the ^{1}H NMR spectra of oligonucleotides, well-established methods utilising both 1D and 2D NMR experiments are available to facilitate the

complete assignment of the proton resonances of short oligonucleotide chains. [5, 9, 93, 94] As illustrated in Figure 4.1, the resonances of particular sugar and base protons of a given oligonucleotide may be found in well-defined chemical shift regions of the ^{1}H NMR spectrum.

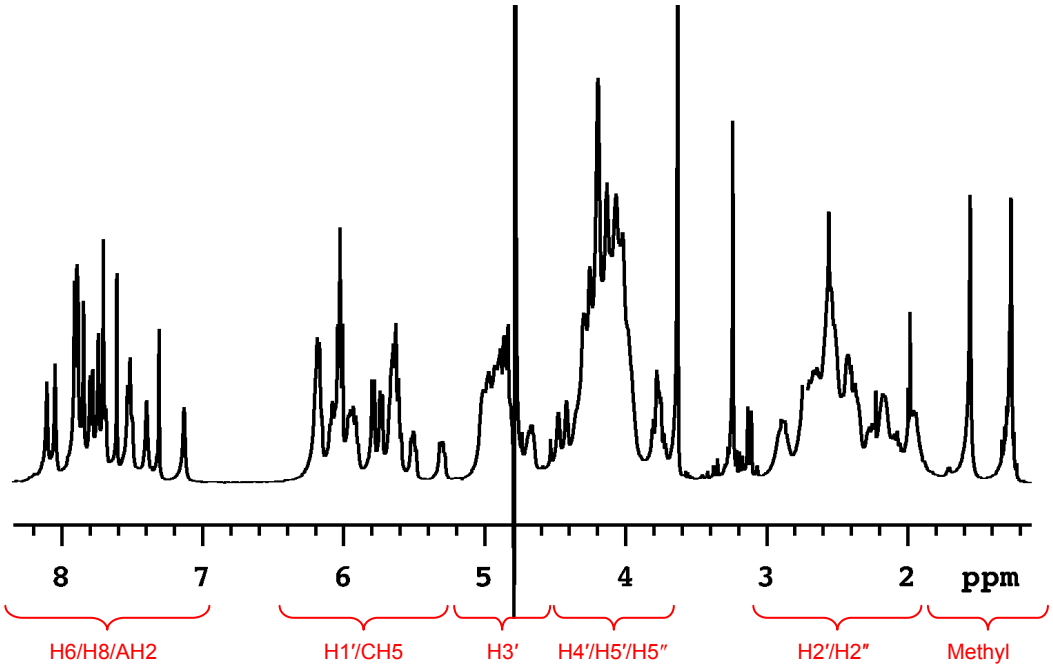

Figure 4.1
The characteristic proton resonances of an oligodeoxyribonucleotide. Pictured here is the ^{1}H NMR spectrum of the bulge-containing tridecanucleotide d(CCG**A**GAATTCCGG)$_2$ in D_2O at 25 ºC. Regions corresponding to characteristic sugar and base proton resonances are labelled.

Further clarification of the ^{1}H NMR spectrum is made by assigning the H6 and H8 proton resonances to their specific bases (A, C, G or T) through the use of several general guidelines:[94]

- Adenine H8 protons experience only small ring currents from neighbouring bases and as a result may be found farthest downfield (i.e. A-H8 protons are the least shielded of all the base protons).

- Guanine H8 proton resonances appear further upfield (typically in the 8.0 to 7.7 ppm range).

- Cytosine and thymine H6 resonances appear farthest upfield (generally in the range of 7.65 to 7.10 ppm).

- Cytosine H6 resonances are spin-coupled to the resonances of the adjacent cytosine H5 protons with a coupling constant of 7.5 Hz. The C-H5 doublets occur much further upfield than do the C-H6 doublets, appearing in the region of 6.5 to 5.5 ppm. It is believed that this notable difference arises from the increased shielding experienced by the C-H5 protons due to their position within the oligonucleotide helix.

- Adenine H2 protons may be assigned through the use of spin-lattice relaxation experiments given that their T_1 relaxation time is significantly longer than that of any other base proton.

Once each resonance has been assigned to a particular type of base proton, the sequence of these bases within the oligonucleotide is established through the use of NOESY, augmented by DQFCOSY, experiments. The "sequential walk" assignment strategy is based upon the NOEs observed between base and sugar protons in an oligonucleotide of the B-type helical conformation:[93, 94]

- Each H6 or H8 base proton should exhibit an NOE to the H1′ proton of the *attached* sugar residue, as well as to the H1′ proton of the sugar in the 5′-direction (the distance to the H1′ proton of the sugar in the 3′-direction exceeds the 4.5 Å threshold in which the nuclear Overhauser effect may typically be measured). An expansion of the region of the NOESY spectrum exhibiting these connectivities allows a line to be traced sequentially through connected bases from the 3′-end to the 5′-end of the duplex, thus assigning each H6/H8/H1′ proton to a specific base in the oligonucleotide sequence. This process is illustrated in Figure 4.2 which shows the connectivies of the d(CCG**A**GAATTCCGG)$_2$ bulge sequence. Contours arising from cytosine H5-H6 interactions are also seen in the NOESY region depicted, as are adenine H2 connectivities.

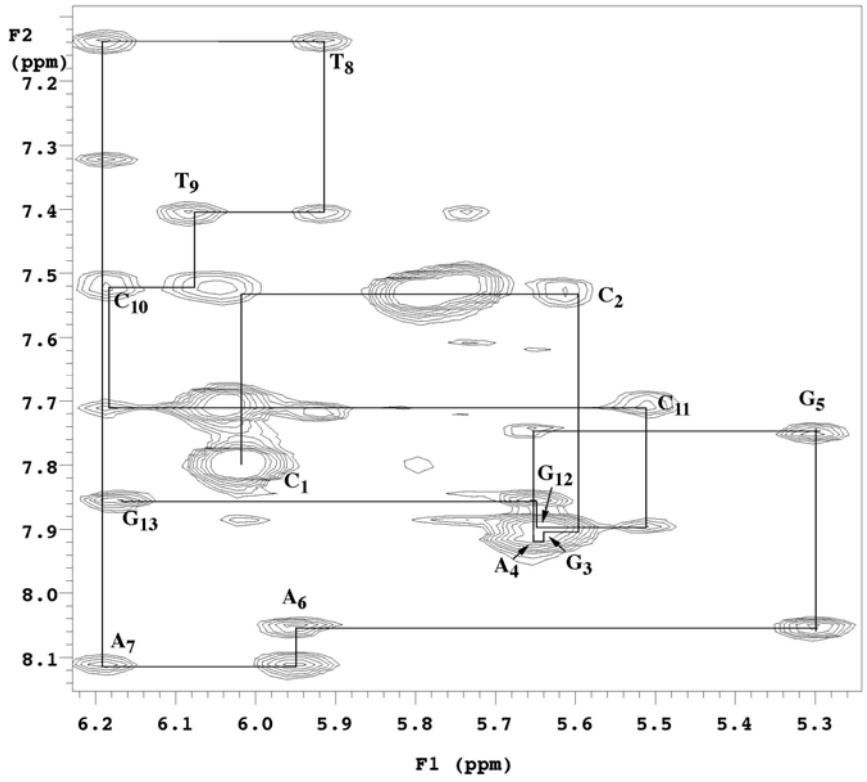

Figure 4.2
The "sequential walk" method of assigning oligonucleotide resonances. Pictured here is the H6/H8 versus H1′/CH5 region of the NOESY spectrum of d(CCG**A**GAATTCCGG)$_2$ in D_2O at 25 ºC with a 350 ms mixing time. A path has been traced sequentially through the contours corresponding to the base sequence of the oligonucleotide.

- In addition to the H1′ protons, each H6/H8 base proton also exhibits NOEs to the H2′ and H2″ protons of both its own sugar residue and that on its 5′-flank. Consequently, the H2′/ H2″ protons can be assigned using the same technique as that for the H1′ protons above, however the region depicting the base-H2′/ H2″ connectivities is somewhat more complicated. Fortunately, COSY spectra may aid in the assignment of the H2′/ H2″ protons which are spin-coupled to the H1′ protons of the same sugar residue (identified by means of the NOESY spectrum). Cross-peaks between thymine methyl-group protons and the H6 proton on both their own and 5′-flanking bases are also observed in the H6/H8 to H2′/ H2″ region of the NOESY spectrum.

- Connectivities between the H6/H8 base protons and H3′ sugar protons may also be observed in the NOESY spectrum, thus facilitating the assignment of H3′ chemical shifts. These assignments may be confirmed by cross-peaks between H3′ and H2′

sugar protons in the COSY spectrum (H3′ to H2″ COSY signals are usually weak in intensity due to the small coupling constants between these protons).

- H4′ sugar protons are assigned primarily through their connectivities to the H3′ sugar protons in the COSY spectrum as they cannot be unambiguously assigned from the NOESY spectrum.

Systematic assignment of proton resonances can therefore usually be used to deduce both the conformation and sequence of a short oligonucleotide of a diverse base composition. In the instances of the bulge-containing oligonucleotide d(CCG**A**GAATTCCGG)$_2$ and its control sequence d(CCGGAATTCCGG)$_2$, the B-type configuration of these duplexes was confirmed and the unpaired adenine bases of the former were found to stack within the helix,[65] consistent with the usual tendency of bulge structures to adopt an intrahelical configuration in solution.[91, 95, 96] Likewise, NMR data advocated B-type helical conformations for the stems of the hairpin loop structures. Base pairing within these helical regions was confirmed by means of observations of guanine and thymine imino proton resonances in NMR experiments conducted in 90% H_2O/10% D_2O. In some instances, terminal imino resonances were weak or only observed at lower temperature due to the inherent "fraying" of short duplex structures.[23] In all instances these B-type conformations were found to be largely unperturbed upon the binding of metal complexes. Chemical shifts of the non-exchangeable protons of the free oligonucleotides are tabulated in Appendix F.

The resonances of the free [d(AT)$_6$]$_2$ dodecanucleotide were found to be unusually broad relative to those of the other oligonucleotide spectra, suggesting an intermediate-exchange between two or more conformations at the temperature of the experiment (25 °C). Indeed, the polymorphism of AT-rich oligonucleotides is well-established, with the variety of solid-state and solution structures reported for such a sequence including A-form,[97] C-form,[98] left-handed,[99, 100] and Hoogsteen base-paired duplexes,[101] as well as coiled coils[102] and hairpin loops.[103] Typically, the reported conformations are variations on the canonical B-DNA duplex,[104-111] most notably the "wrinkled D-DNA" form which features a narrower-than-usual minor groove and alternating torsion angles between AT and TA steps.[105, 112-115] While the precise conformation(s) assumed by the free [d(AT)$_6$]$_2$ oligonucleotide could not be ascertained in the present experiments, the observed pattern of NOE crosspeaks was found to be typical of a

B-type duplex. However, the significant broadening of resonances and an overlap of resonances due to the limited diversity of the base sequence of this oligonucleotide made assignment of all resonances to specific bases within the sequence impossible.

4.3.3 Binding of HAT-Bridged Species to Duplex and Bulge-DNA

Preliminary NMR investigations into the binding of HAT-bridged species, conducted prior to initial FID assays, were undertaken with the aim of studying the effect of a change in bridging ligand. Thus, $[\{Ru(Me_2bpy)_2\}_2(\mu\text{-HAT})]^{4+}$ and $[\{Ru(bpy)_2\}_2(\mu\text{-HAT})]^{4+}$ were used to probe the same bulge sequence, d(CCG**A**GAATTCCGG)$_2$, to which the bpm-bridged species $[\{Ru(Me_2bpy)_2\}_2(\mu\text{-bpm})]^{4+}$ was found to bind with total enantioselectivity.[65, 66]

Initially, and not unexpectedly, ΔΔ-$[\{Ru(Me_2bpy)_2\}_2(\mu\text{-HAT})]^{4+}$ was found to associate poorly with the bulge-free control sequence d(CCGGAATTCCGG)$_2$. Metal complex resonances exhibited fairly uniform small-to-moderate upfield shifts (*ca.* 0.05-0.10 ppm), similar in magnitude to those exhibited by ΔΔ-$[\{Ru(Me_2bpy)_2\}_2(\mu\text{-bpm})]^{4+}$ upon binding to the same oligonucleotide.[65] There was no significant broadening of the single set of metal complex resonances, suggesting binding kinetics in the fast-exchange regime. Upon the binding of ΔΔ-$[\{Ru(Me_2bpy)_2\}_2(\mu\text{-HAT})]^{4+}$ the oligonucleotide resonances remained relatively unperturbed with only some minor changes in the chemical shifts of resonances relating to the terminal residues of the oligonucleotide. Furthermore, the few intermolecular NOE signals seen in NOESY spectra were mostly weak correlations between the metal complex and the ends of the duplex. These observations reaffirm the notion that bulky dinuclear complexes bind weakly to duplex DNA; in this instance the complex appears to favour the ends of the oligonucleotide where, presumably, fraying of the duplex creates a more accommodating binding site.

Upon binding to the bulge-containing oligonucleotide d(CCG**A**GAATTCCGG)$_2$, both the ΔΔ and ΛΛ enantiomers of $[\{Ru(Me_2bpy)_2\}_2(\mu\text{-HAT})]^{4+}$ exhibit a single set of NMR resonances with some increase in line width (particularly in the H3/H3′ protons of Me_2bpy rings *a* and *b* – see Chapter 2 for ligand and ring notation), suggesting intermediate-to-fast binding kinetics. A few metal complex resonances underwent very small upfield shifts (ΔΔ moreso than ΛΛ), however these shifts were smaller than those exhibited by ΔΔ-$[\{Ru(Me_2bpy)_2\}_2(\mu\text{-HAT})]^{4+}$ upon binding to the control oligonucleotide and much less significant than those seen in the spectrum of ΔΔ-$[\{Ru(Me_2bpy)_2\}_2(\mu\text{-bpm})]^{4+}$ binding to the

bulge sequence. Likewise, the spectrum of the oligonucleotide underwent minimal change upon binding of either enantiomer, with the exception of base and sugar proton resonances relating to the A_4 residue. Being the unpaired base, A_4 lacks stabilising hydrogen-bonding and is therefore more readily perturbed upon the binding of metal complexes to the duplex, although not necessarily directly to the bulge site. Both enantiomers demonstrated a few relatively strong NOEs to resonances belonging to trityl group impurities present in the spectrum of the bulge oligonucleotide. These protecting groups, carried over from the synthesis of the duplex, are located on the 5′-ends of each strand; NOEs to these signals suggest that the metal complex is again preferentially binding at the frayed termini of the duplex. Nevertheless, the ΔΔ enantiomer did exhibit a few additional NOEs of moderate strength to residues in the proximity of the bulge site (specifically, cross-peaks between H*b* and H*c* HAT ligand protons and the H1′ sugar protons of G_5 and A_6). While this is indicative of a small enantioselective preference of the ΔΔ enantiomer for the bulge site, the bulk of the data is suggestive of a relatively poor affinity by the HAT complexes for this oligonucleotide. By monitoring systematic shifts in metal complex resonances throughout NMR titrations and applying Equation 4.3 it was possible to estimate an association constant for the binding of ΔΔ-$[\{Ru(Me_2bpy)_2\}_2(\mu\text{-HAT})]^{4+}$ to the bulge-containing oligonucleotide: 1-2 × 10^4 M^{-1}. Shifts in the resonances of the ΛΛ enantiomer were insufficient to estimate a binding constant.

Rudimentary modelling of the association between ΔΔ-$[\{Ru(Me_2bpy)_2\}_2(\mu\text{-HAT})]^{4+}$ and the bulge-containing oligonucleotide implied that the optimal orientation of the HAT-bridged complex is “tail-in” (see Figure 4.3). This model has the metal-free end of the HAT ligand inserted into the minor groove with rings *a* and *b* of the Me_2bpy ligands sitting against the phosphate backbone on either side of the minor groove. Steric interactions prevent a deep insertion of the HAT ligand, explaining the relatively poor association of the complex with the oligonucleotide (presumably the incompatible chirality of the ΛΛ enantiomer aggravates these steric clashes, resulting in weaker association). Such a binding mode is supported by NOE data implying close contacts between minor groove sugar protons and the H*b*/H*c* protons on the metal-free tail end of the HAT ligand, and line broadening of the H3/H3′ Me_2bpy resonances of rings *a* and *b* which would be subjected to significant steric interactions in such an orientation.

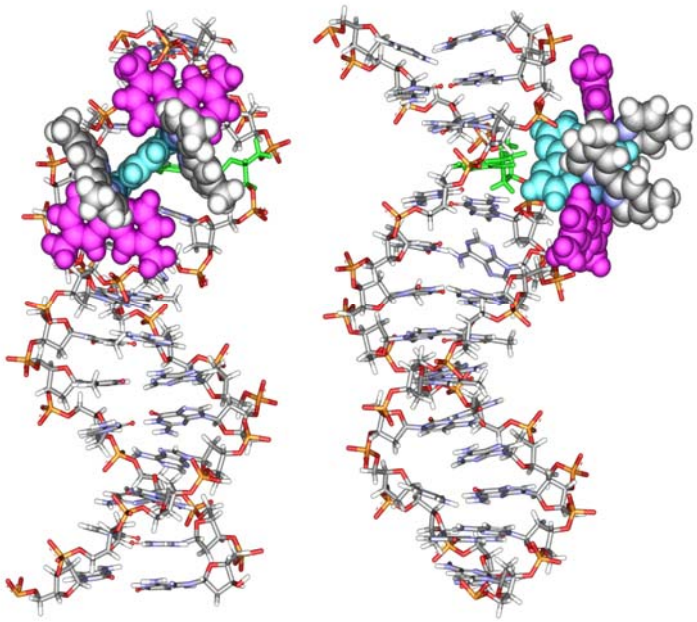

Figure 4.3
The binding of HAT-bridged complexes to a single-base bulge site. This model illustrates the association between ΔΔ-[{Ru(Me_2bpy)$_2$}$_2$(μ-HAT)]$^{4+}$ and the bulge site of the tridecanucleotide d(CCG**A**GAATTCCGG)$_2$ from two different angles. The metal complex binds via a "tail-first" insertion of the HAT ligand (rendered in light blue), however deep binding is prevented by steric clashes with the terminal ligands depicted in purple. The unpaired adenosine nucleotide at the binding site is rendered in green.

The HAT-bridged complex possessing non-methylated bipyridine terminal ligands, ΔΔ-[{Ru(bpy)$_2$}$_2$(μ-HAT)]$^{4+}$, exhibited a single set of metal complex resonances with no appreciable line-width broadening upon binding to the bulge-containing oligonucleotide; however, the resonances of the complex did undergo relatively large upfield shifts of approximately 0.05 to 0.15 ppm. Overall, these shifts were larger than those experienced by either enantiomer of [{Ru(Me_2bpy)$_2$}$_2$(μ-HAT)]$^{4+}$ or by ΔΔ-[{Ru(Me_2bpy)$_2$}$_2$(μ-bpm)]$^{4+}$ upon binding to the same oligonucleotide. A binding constant of 1×10^4 M^{-1} was estimated from these shifts. The spectrum of the oligonucleotide underwent negligible perturbation from that of its free state; even resonances from the A_4 residue were largely unchanged upon binding of the metal complex, contrasting to the case in which [{Ru(Me_2bpy)$_2$}$_2$(μ-HAT)]$^{4+}$ was added to this oligonucleotide. Few notable intermolecular NOEs were observed, other than some weak correlations to minor groove H1′ protons. Given that relatively large chemical shift changes in the metal complex spectrum are not supported by any corresponding changes in the oligonucleotide spectrum nor any significant NOEs, it might be concluded that the metal complex is binding to the oligonucleotide with limited specificity. It appears that the methyl

groups on the terminal ligands of $[\{Ru(Me_2bpy)_2\}_2(\mu\text{-HAT})]^{4+}$ confer upon this complex slower binding kinetics due to its increased bulk and/or enhanced van der Waals and hydrophobic interactions; an oligonucleotide-metal complex association which is longer on the NMR timescale typically yields more intense NOEs. Conversely, the lack of specificity observed in the non-methylated species suggests a largely electrostatic association between itself and the polyanionic backbone of the oligonucleotide, with NOE data implying limited occupation of the minor groove.

4.3.4 Binding of HAT-Bridged Species to a 4-Base Hairpin Loop

As a general confirmation of the validity of the FID assay, the binding of ΔΔ-$[\{Ru(bpy)_2\}_2(\mu\text{-HAT})]^{4+}$ to an octadecanucleotide containing a 4-base hairpin loop and 7-base pair stem, d(CACTGGT**CTCT**ACCAGTG), was examined. In the FID assay, addition of ΔΔ-$[\{Ru(bpy)_2\}_2(\mu\text{-HAT})]^{4+}$ to the octadecanucleotide resulted in a fluorescence decrease of only 12%, indicative of weak binding by the ruthenium complex to this particular sequence. Upon titration of ΔΔ-$[\{Ru(bpy)_2\}_2(\mu\text{-HAT})]^{4+}$ into the octadecanucleotide, small upfield shifts of most of the metal complex resonances were observed in the NMR spectra albeit with little broadening, suggesting binding kinetics in the fast-exchange regime. Furthermore, the binding of the metal complex induced negligible change in chemical shift or broadening of the oligonucleotide resonances. Also, the only NOEs observed in NOESY spectra were very weak cross-peaks to the terminal residues in the stem of the hairpin loop. As with the double-stranded species described above, it is believed that the metal complex bound weakly to the octadecanucleotide, specifically at the potentially frayed end of the duplex stem. The binding behaviour observed in these NMR experiments is consistent with the relatively poor binding affinity implied by the FID assay.

4.3.5 Binding of HAT-Bridged Species to a 6-Base Hairpin Loop

The results of ethidium bromide-based FID assay highlighted a particular affinity of the $[\{Ru(phen)_2\}_2(\mu\text{-HAT})]^{4+}$ and $[\{Ru(Me_2phen)_2\}_2(\mu\text{-HAT})]^{4+}$ complexes for the 6-base hairpin loop icosanucleotide d(CACTGGT**CTCTCT**ACCAGTG). As was generally the case for the angular-bridged complexes, it was the *meso* isomers that demonstrated the greatest apparent

affinity (i.e. they induced the greatest decrease in fluorescence in the FID assay). The FID assay also implied that while $[\{Ru(Me_2phen)_2\}_2(\mu\text{-HAT})]^{4+}$ was the stronger binder, $[\{Ru(phen)_2\}_2(\mu\text{-HAT})]^{4+}$ possessed a higher selectivity by more readily distinguishing between oligonucleotides. NMR experiments were conducted with each metal complex to further elucidate the nature of their interactions with the 6-base hairpin loop (for further details on the FID assays refer to Chapter 3).

As depicted in Figure 4.4, the addition of *meso*-$[\{Ru(phen)_2\}_2(\mu\text{-HAT})]^{4+}$ to the 6-base hairpin loop sequence induced selective broadening of the T_7 and T_{13} methyl resonances, and to a lesser extent the T_9 methyl resonance; the T_4, T_{11} and T_{19} resonances remained relatively unaffected. Figure 4.5 illustrates the relative positions of each of these thymine residues within the icosanucleotide; those resonances undergoing broadening lay at or near the stem-loop interface, implying that this is where the metal complex is binding. Addition of *meso*-$[\{Ru(Me_2phen)_2\}_2(\mu\text{-HAT})]^{4+}$ to the icosanucleotide induced a similar effect to the non-methylated analogue, albeit at lower molar ratios (refer to Figure 4.6) suggesting stronger binding. Again, the T_7, T_{13} and T_9 methyl resonances underwent selective broadening, as did the methyl resonance of the T_{11} residue (located at the apex of the loop) to a lesser extent. The T_4 and T_{19} methyl resonances remained largely unaffected.

The binding of these metal complexes at the stem-loop interface or within the loop of the icosanucleotide is further supported by selective disappearance of cytosine H5-H6 cross-peaks in DQFCOSY spectra due to line-broadening induced cancellation of anti-phase components. In DQFCOSY spectra of either ruthenium complex at a 1:1 ratio with the icosanucleotide the cytosine H5-H6 cross-peaks of those residues in the duplex (stem) region of the oligonucleotide were clearly visible, whereas the corresponding cross-peaks from cytosine residues in the loop region were not observed (or were extremely weak) at 25 or 40 °C.

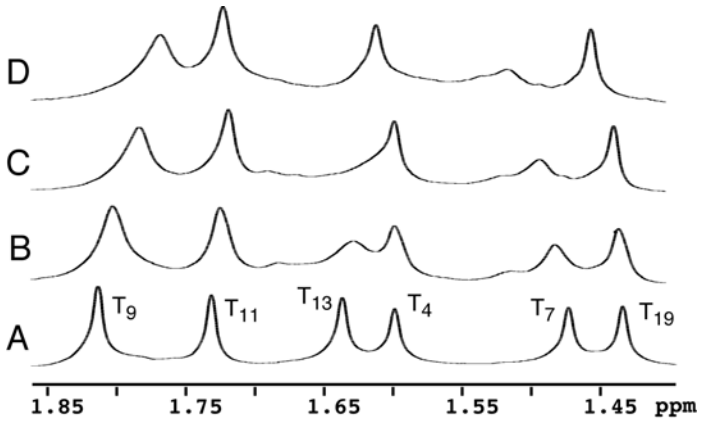

Figure 4.4
Selective thymine methyl resonance broadening upon the addition of *meso*-[{Ru(phen)$_2$}$_2$(μ-HAT)]$^{4+}$ to d(CACTGGTCTCTCTACCAGTG). NMR spectra of the T-methyl region of **(A) t**he free 6-base hairpin icosanucleotide, and with added *meso*-[{Ru(phen)$_2$}$_2$(μ-HAT)]$^{4+}$ at metal complex-to-icosanucleotide ratios of **(B)** 0.25, **(C)** 0.60, and **(D)** 1.0.

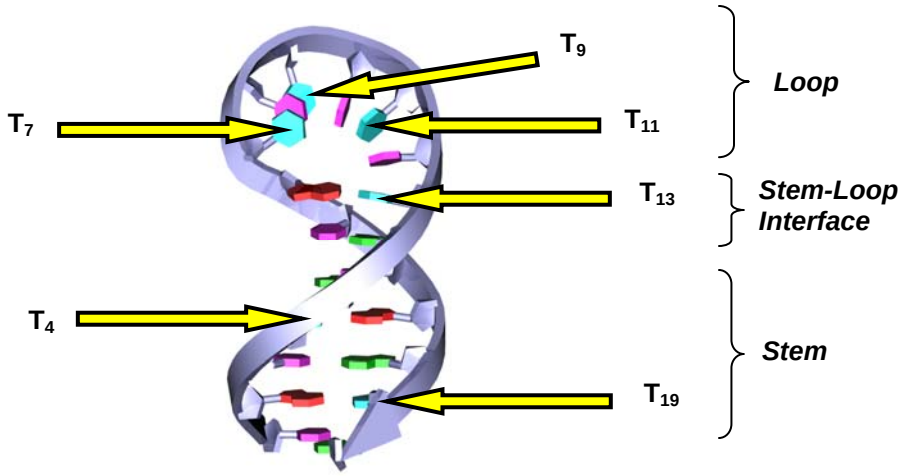

Figure 4.5
Thymine residues in the 6-base hairpin loop sequence d(CACTGGTCTCTCTACCAGTG). This schematic representation of the hairpin loop illustrates the relative locations of all the thymine residues (rendered light blue).

Observations of the aromatic region of the ^{1}H NMR spectrum of the icosanucleotide with added metal complex revealed selective broadening of several icosanucleotide proton resonances (see Figure 4.7). The A_{14}-H8, A_{14}-H2 and T_7-H6 resonances were seen to significantly broaden when titrated with either *meso*-[{Ru(phen)$_2$}$_2$(μ-HAT)]$^{4+}$ or *meso*-[{Ru(Me$_2$phen)$_2$}$_2$(μ-HAT)]$^{4+}$. The effect was more prominent upon addition of the latter metal complex, with each of the resonances broadening to such an extent as to make them very difficult to locate within the spectrum at mid-to-high metal complex-to-icosanucleotide ratios. In the *meso*-[{Ru(phen)$_2$}$_2$(μ-HAT)]$^{4+}$ titration this magnitude of broadening was only observed

with the A_{14}-H2 resonance. Some broadening and a small downfield shift were seen for the T_{13}-H6 resonance in the presence of each of the metal complexes, while the C_8-H6 and C_{10}-H6 doublets underwent small upfield shifts and minor broadening in the presence of *meso*-$[\{Ru(phen)_2\}_2(\mu\text{-HAT})]^{4+}$ and *meso*-$[\{Ru(Me_2phen)_2\}_2(\mu\text{-HAT})]^{4+}$, respectively. These perturbations to icosanucleotide resonances at and around the stem-loop interface are indicative of selective binding by the ruthenium complexes at this specific site.

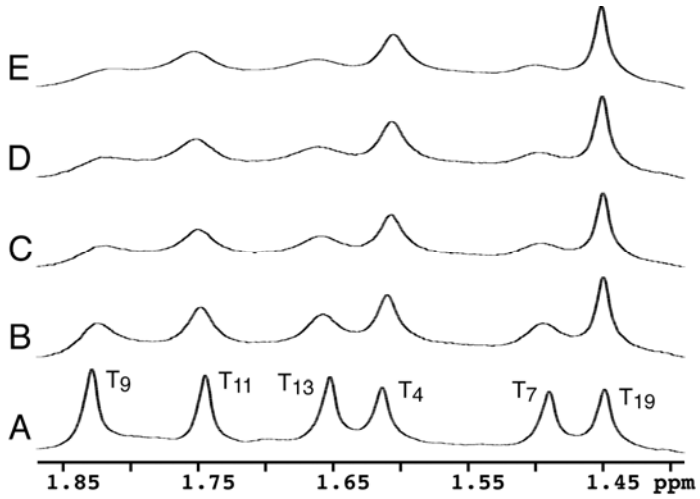

Figure 4.6
Selective thymine methyl resonance broadening upon the addition of *meso*-$[\{Ru(Me_2phen)_2\}_2(\mu\text{-HAT})]^{4+}$ to d(CACTGGTCTCTCTACCAGTG). NMR spectra of the T-methyl region of **(A) t**he free 6-base hairpin icosanucleotide, and with added *meso*-$[\{Ru(Me_2phen)_2\}_2(\mu\text{-HAT})]^{4+}$ at metal complex-to-icosanucleotide ratios of **(B)** 0.10, **(C)** 0.15, **(D)** 0.20, and **(E)** 0.50.

Addition of either ruthenium complex to the icosanucleotide induced selective broadening of the metal complex peaks, with resonances from *meso*-$[\{Ru(Me_2phen)_2\}_2(\mu\text{-HAT})]^{4+}$ broadening to a greater degree than those of the non-methylated analogue. Due to the extent of the broadening it was not possible to unambiguously assign all the metal complex resonances at temperatures below 60 °C. Such broadening, indicative of binding kinetics in the intermediate exchange regime, implies strong binding by the metal complexes. As has previously been seen in studies of the interaction of *meso* dinuclear complexes with DNA,[60, 66] two sets of resonances were detected (although only clearly distinguished at temperatures > 40 °C for the methylated analogue) for each metal complex upon binding to the oligonucleotide. This double set of resonances is most likely attributed to the differing binding natures of the Δ and Λ ends of the metal complex. Significant upfield shifts (> 0.2 ppm) were observed for phen H3/H8

resonances of both metal complexes upon binding to the icosanucleotide. No significant shifts were observed for resonances from the HAT ligand of *meso*-[{Ru(phen)$_2$}$_2$(μ-HAT)]$^{4+}$ whereas the HAT H*b* and H*c* resonances of the methylated analogue were seen to undergo downfield shifts of approximately 0.2 ppm.

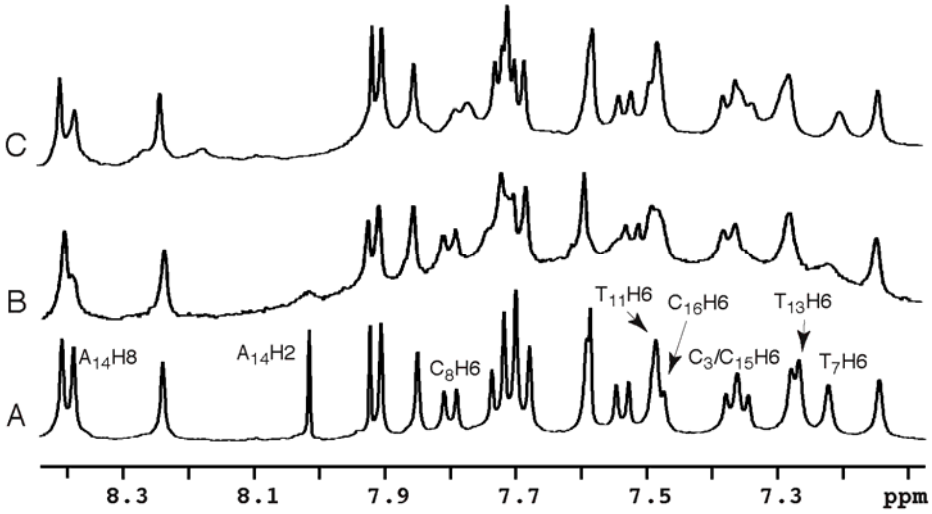

Figure 4.7
Aromatic proton resonance broadening of a 6-base hairpin loop sequence upon the binding of *meso*-[{Ru(phen)$_2$}$_2$(μ-HAT)]$^{4+}$ and *meso*-[{Ru(Me$_2$phen)$_2$}$_2$(μ-HAT)]$^{4+}$. NMR spectra of the aromatic region of the free 6-base hairpin icosanucleotide d(CACTGGT**CTCTCT**ACCAGTG) **(A)**, and with added *meso*-[{Ru(Me$_2$phen)$_2$}$_2$(μ-HAT)]$^{4+}$ **(B)** and *meso*-[{Ru(phen)$_2$}$_2$(μ-HAT)]$^{4+}$ **(C)** at metal complex-to-icosanucleotide ratios of 0.10 and 0.30, respectively.

NOESY spectra of both *meso*-[{Ru(phen)$_2$}$_2$(μ-HAT)]$^{4+}$ and *meso*-[{Ru(Me$_2$phen)$_2$}$_2$(μ-HAT)]$^{4+}$ bound to the 6-base hairpin icosanucleotide were recorded at a range of temperatures at both 400 and 800 MHz. Due to the extensive broadening of both metal complex and icosanucleotide resonances, little binding information could be acquired from the NOESY spectra. Although few intermolecular NOEs could be unambiguously assigned, the results are consistent with the proposal that the ruthenium complexes bind the icosanucleotide at the stem-loop interface: *meso*-[{Ru(phen)$_2$}$_2$(μ-HAT)]$^{4+}$ exhibited a few weak NOEs from the metal complex to T$_7$H1′ and T$_7$H2″ icosanucleotide proton resonances (see Figure 4.8), and each of the ruthenium complexes exhibited a number of weak NOEs to the H4′ protons of nucleotides tentatively identified as G$_6$, T$_7$ and A$_{14}$. Intriguingly, while NOEs to H1′ and H4′ sugar proton resonances are consistent with a minor groove-binding mode, the H2″ sugar protons are typically orientated into the *major* groove.

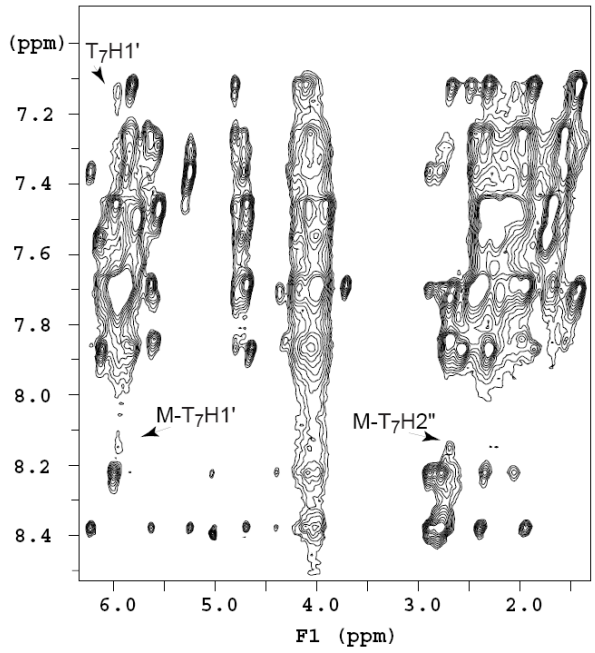

Figure 4.8
NOESY spectrum expansion of *meso*-[{Ru(phen)$_2$}$_2$(μ-HAT)]$^{4+}$ bound to the icosanucleotide d(CACTGGTCTCTCTACCAGTG). Spectrum obtained with a 300 ms mixing time at 10 °C, with a metal complex-to-icosanucleotide ratio of 1.0. Labelled in the spectrum are several notable connectivities between metal complex aromatic protons and the T_7H1' and T_7H2'' resonances of the icosanucleotide.

Since only exchange-averaged resonances were observed in the spectra of the icosanucleotide with added metal complex, a quantitative binding model could not be established from NOE-constrained molecular dynamics calculations. However, using observed NOEs as a guide, simple molecular mechanics-based models were constructed using the program HyperChem.[83] These models provided some means of comparing and contrasting the potential binding sites of *meso*-[{Ru(phen)$_2$}$_2$(μ-HAT)]$^{4+}$ and *meso*-[{Ru(Me$_2$phen)$_2$}$_2$(μ-HAT)]$^{4+}$ complexes, as well as giving an insight into the preferential binding of the *meso* diastereoisomer of the HAT-bridged complexes over either enantiomeric form. As each complex is comprised of conjugated aromatic rings which are structurally rigid when coordinated, it was treated as a rigid entity around which the icosanucleotide model was allowed to optimise its structure. For the relatively simple multiply-bonded structures this represents a reasonable approximation that does allow a comparison of a range of physically-plausible binding models. Numerous energy minimisations were made with minor alternations to the starting orientations of the metal complexes in order to examine a wide range of binding modes. The minimum-energy binding models of the *meso*-[{Ru(phen)$_2$}$_2$(μ-HAT)]$^{4+}$ and *meso*-

$[\{Ru(Me_2phen)_2\}_2(\mu\text{-HAT})]^{4+}$ complexes with the 6-base hairpin icosanucleotide are described below.

The *meso*-$[\{Ru(phen)_2\}_2(\mu\text{-HAT})]^{4+}$ metal complex was manually docked in the minor groove side of the icosanucleotide, consistent with the NOEs observed to H4′ and H1′ proton resonances. Energy minimisations were performed from several starting sites along the length of the minor groove (and the corresponding side of the hairpin loop). The lowest-energy association, depicted in Figure 4.9, was found to occur with the bulk of the metal complex adjacent to the bases of the stem-loop interface (again consistent with NOEs observed to T_7 protons, as well as the selective broadening of resonances observed in one-dimensional spectra). In this model the HAT bridging ligand lies flat across the minor groove at the stem-loop interface, with the two terminal ligands making up the long axis of the metal complex projecting into the groove of the stem and adjacent loop region. Such an arrangement best satisfies the observed NOEs to T_7 protons at the hairpin stem, as well as the selective broadening of T_{13} methyl resonances within the loop region; however, it is a considerably different orientation than in the models of the similar HAT-bridged complexes bound to the bulge-containing tridecanucleotide d(CCG**A**GAATTCCGG)$_2$, as seen above. The remaining two phen ligands, roughly orthogonal to the long axis of the metal complex, are positioned across the minor groove in the direction of the loop. Such an orientation removes these ligands from solution to some degree, facilitating more favourable hydrophobic interactions with the DNA. The observation of NOEs to both T_7H1′ and T_7H2″ concurs with such an arrangement: since H1′ and H2″ are not normally exposed to the same groove, these NOEs may be most likely attributed to orthogonal ligands. Given that the T_7H2″ proton is located closer to the loop region than is the T_7H1′ proton, the NOE signals of the former are likely to have formed with the ligands of the long axis as these ligands are located nearer to the centre of the metal complex.

A potential alternative arrangement exists in which the metal complex is rotated about a central axis perpendicular to the plane of the HAT ligand. Such a model has the complex bound at the same position but with the phen ligands orthogonal to the long axis of the complex, projecting away from the loop region into solution. In this orientation the phen ligands of the long axis neatly follow the contour of the minor groove; however geometry optimisation reveals this model to have a modest energy disadvantage (approximately 3 kcal mol^{-1}) over its

counterpart, most likely due to less favourable interactions from the ligands now projecting into solution.

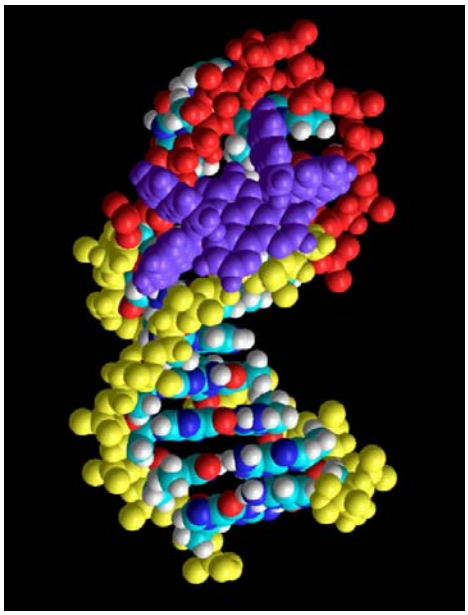

Figure 4.9
Model of *meso*-[{Ru(phen)$_2$}$_2$(μ-HAT)]$^{4+}$ bound to the 6-base hairpin loop icosanucleotide d(CACTGGTCTCTCTACCAGTG). Energy minimised HyperChem model; the metal complex (purple) is bound at the stem-loop interface of the icosanucleotide. The phosphate backbone of the duplex region of the DNA is depicted in yellow, the loop region in red.

Models of the analogous metal complex with methylated terminal ligands, *meso*-[{Ru(Me$_2$phen)$_2$}$_2$(μ-HAT)]$^{4+}$, suggest that this complex binds to the icosanucleotide at the same stem-loop interface as does the non-methylated analogue. This position is again supported by NOE signals (to G_6, T_7 and A_{14} proton resonances) and selective broadening of stem-loop T-methyl resonances. Interestingly, both of the geometry-optimised orientations described above for the non-methylated metal complex yield equivalent energy minima for *meso*-[{Ru(Me$_2$phen)$_2$}$_2$(μ-HAT)]$^{4+}$. Each of these orientations is depicted in Figure 4.10. It is possible that the effect of projecting the Me$_2$phen ligands orthogonal to the long axis of the complex into solution is counteracted by additional hydrophobic interactions within the loop region upon accommodating the increased bulk of the methyl substituents. As a result, the methylated species may potentially bind in both orientations. This rationale may explain the reduced selectivity observed in the broadening of T-methyl resonances in the loop region on the addition of the methylated species: within this region broadening due to the addition of *meso*-[{Ru(phen)$_2$}$_2$(μ-HAT)]$^{4+}$ was largely confined to the T_{13}-methyl resonance, whereas *meso*-

[{Ru(Me$_2$phen)$_2$}$_2$(μ-HAT)]$^{4+}$ also induced significant broadening in the T$_9$-methyl resonance and, to a lesser extent, the T$_{11}$-methyl resonance. A superficial examination of these models reveals the apparent reason for the higher affinity exhibited by the *meso* diastereoisomer: as seen in Figures 4.9 and 4.10, the phen ligands atop the plane of the bridging ligand (if the viewer is considered to be looking "down" onto the metal complex) are orientated almost perpendicular to the minor groove whereas those underneath the plane of the ligand run along the length of the groove. In either homochiral dinuclear species one of the *underside* phen ligands would be orientated perpendicular to the groove, inducing significant (and presumably unfavourable) steric clashes. Thus, the *meso* diastereoisomer appears to be better accommodated by the curvature of the narrow minor groove.

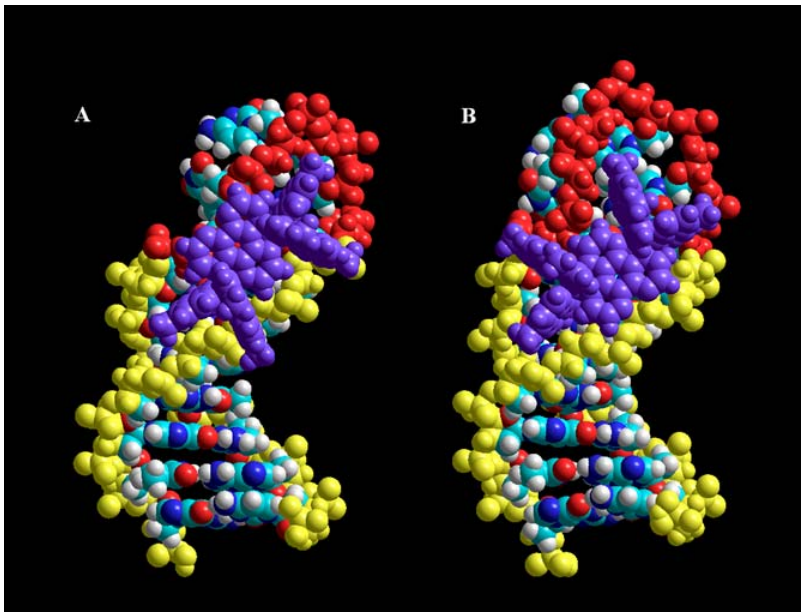

Figure 4.10
Two models of *meso*-[{Ru(Me$_2$phen)$_2$}$_2$(μ-HAT)]$^{4+}$ bound to the 6-base hairpin loop icosanucleotide d(CACTGGTCTCTCTACCAGTG). Energy minimised HyperChem model; the metal complex (purple) is bound at the stem-loop interface of the icosanucleotide. The phosphate backbone of the duplex region of the DNA is depicted in yellow, the loop region in red. Orientations A and B possessed identical energy minima.

It is evident from the observations of selective broadening of T-methyl proton resonances and intermolecular NOEs to specific icosanucleotide residues that both of the metal complexes, *meso*-[{Ru(phen)$_2$}$_2$(μ-HAT)]$^{4+}$ and *meso*-[{Ru(Me$_2$phen)$_2$}$_2$(μ-HAT)]$^{4+}$, bind at the stem-loop interface on the minor groove-side of the icosanucleotide. This site is most likely wider, or at least more flexible, than the duplex stem of the icosanucleotide, while still offering

energetically favourable van der Waals and hydrophobic interactions with the bulky dinuclear complexes. These suppositions are consistent with observations that dinuclear complexes such as these bind in the minor groove, but will preferentially target more open regions of the groove in order to accommodate their increased steric bulk.[65, 66, 72, 74] Indeed, NMR studies conducted into the binding of the mononuclear complex $[Ru(bpy)_2(bbtb)]^{2+}$ {4,4′-bis(benzothiazol-2-yl)-2,2′-bipyridine} with the same hairpin loop-containing octadecanucleotide and icosanucleotide also indicate that the stem-loop interface was again the preferred binding site.[116] In that example, molecular models based on NMR data place the cationic ruthenium centre just within the duplex stem while one of the large non-polar benzothiazole substituents projects into the loop region where it is shielded from the solvent.

Of the two metal complexes, *meso*-$[\{Ru(Me_2phen)_2\}_2(\mu\text{-HAT})]^{4+}$ was found to induce more significant broadening of icosanucleotide proton resonances, and at lower molar ratios, than its non-methylated analogue. This may be interpreted as stronger binding by the methylated species, a common observation in DNA-binding studies of polypyridyl transition metal complexes.[69, 70] Secretion of these hydrophobic methyl groups in the minor groove, and the subsequent displacement of solvent, is clearly a major driving force behind the greater binding ability of the methylated species. The general trend of methyl substituents resulting in a greater binding affinity is reflected in FID results, as described in Chapter 3. Unfortunately, while *meso*-$[\{Ru(Me_2phen)_2\}_2(\mu\text{-HAT})]^{4+}$ was found to be a stronger binder than *meso*-$[\{Ru(phen)_2\}_2(\mu\text{-HAT})]^{4+}$ FID results suggest that this greater affinity comes at the cost of selectivity: *meso*-$[\{Ru(Me_2phen)_2\}_2(\mu\text{-HAT})]^{4+}$ binds strongly to most of the oligonucleotides surveyed, whereas *meso*-$[\{Ru(phen)_2\}_2(\mu\text{-HAT})]^{4+}$ exhibits a particular affinity for the 6-base hairpin loop-containing icosanucleotide, making it a potential basis for a high affinity DNA hairpin probe.

4.3.6 Binding of ppz-Bridged Species to an AT Duplex

Like their HAT-bridged counterparts, ppz-bridged species – particularly those with phen or Me_2phen terminal ligands – also demonstrated a particular affinity and selectivity for the larger bulge sites (specifically the 5-base bulges) and hairpin loops (6-base loops > 4-base loops) in FID assays (see Chapter 3 for further details). These similarities were not unexpected given the similarity between the bridging ligands (and, hence, the overall shape of the complexes);

however, the unusually high affinity of the ppz-bridged complexes for the AT duplex sequence $[d(AT)_6]_2$ was unexpected. Most of the metal complexes surveyed demonstrated a greater affinity for $[d(AT)_6]_2$ than they did for any of the other "canonical" duplex sequences, notably a GC-rich sequence and the mixed-sequence bulge control dodecanucleotide; however, the complexes *meso*-$[\{Ru(phen)_2\}_2(\mu\text{-ppz})]^{4+}$ and *meso*-$[\{Ru(Me_2phen)_2\}_2(\mu\text{-ppz})]^{4+}$ appeared to have a greater affinity to the AT sequence than any other oligonucleotide, including the bulges and hairpins. Once again, the *meso* diastereoisomers seemed to be more potent binders than their enantiomeric counterparts ($\Delta\Delta$ and $\Lambda\Lambda$). Furthermore, the interactions between these ppz-bridged complexes and $[d(AT)_2]_6$ were amongst the most impressive in the entire FID assay. It is well-established that AT-rich sites present particularly attractive binding sites for cationic metal complexes due to the greater electronegative charge associated with such sequences;[117] however, the narrower minor groove – particularly in a duplex-only sequence such as that studied here – would seemingly present a less favourable binding site for a bulky dinuclear complex. In order to gain some insight into this apparent contradiction, NMR experiments were conducted in which the binding of *meso*-$[\{Ru(phen)_2\}_2(\mu\text{-ppz})]^{4+}$ to the AT dodecanucleotide $[d(AT)_6]_2$ was probed. This metal complex was chosen in preference to the methylated analogue, *meso*-$[\{Ru(Me_2phen)_2\}_2(\mu\text{-ppz})]^{4+}$, because it was thought that the latter would be an exceptionally strong binder (as implied by FID assays), resulting in significant broadening of NMR resonances and the associated loss of potential NOE binding data in NOESY spectra.

Unfortunately, as described above, proton resonances for the AT dodecanucleotide were unusually broad due to unspecified conformational transitions {see Figure 4.11(A)}, thus preventing the unambiguous assignment of individual resonances. Upon the addition of *meso*-$[\{Ru(phen)_2\}_2(\mu\text{-ppz})]^{4+}$ the oligonucleotide resonances broadened to an even greater extent {see Figure 4.11(B)}, suggesting intermediate exchange kinetics consistent with strong binding by the metal complex. Significant broadening of metal complex resonances was also evident upon addition to the dodecanucleotide, as was some splitting of the symmetry of the metal complex peaks {H*b*, for example – see Figure 4.11(C)}. The latter may be attributed to the non-equivalence of the Δ and Λ chiral metal centres of the *meso* diastereoisomer in this binding environment. Several metal complex resonances, tentatively assigned to the H7, H8 and H9 protons of phenanthroline *ring d*, undergo large upfield shifts. H8d in particular undergoes a very large shift of 0.61 ppm. In this context shifts of this magnitude are often associated with intercalation[118] – a binding mode not usually evident in the interaction of dinuclear metal

complexes of this type – but there are examples of groove-binding species also inducing such large shifts.[72]

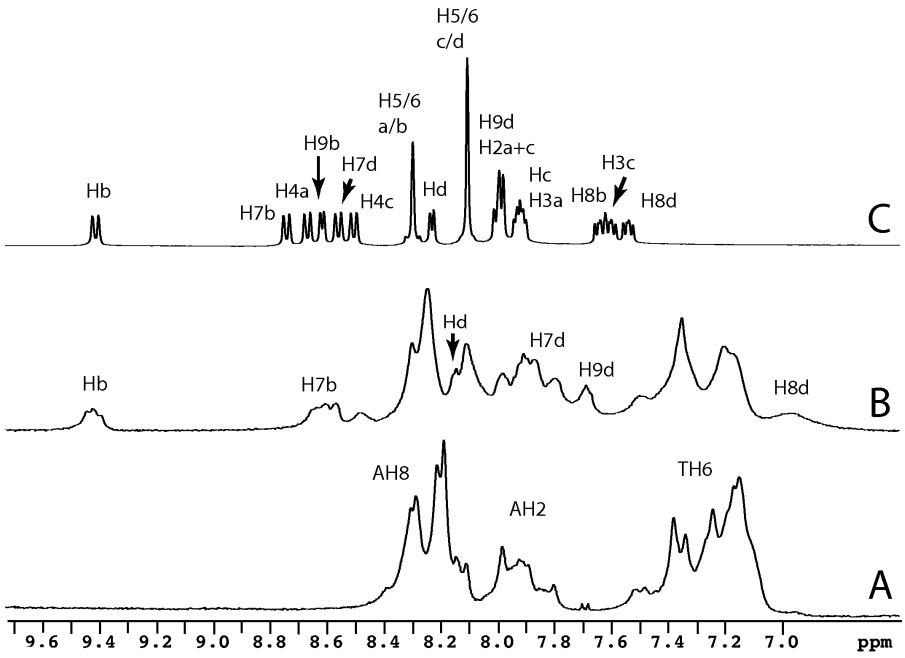

Figure 4.11
Significant broadening and upfield shifts of resonances upon the binding of *meso*-[{Ru(phen)$_2$}$_2$(μ-ppz)]$^{4+}$ to the dodecanucleotide [d(AT)$_6$]$_2$. ^{1}H NMR spectra (25 °C) of the free oligonucleotide **(A)**, a 1:1 mixture of the metal complex and oligonucleotide **(B)**, and the free metal complex **(C)**.

NOESY spectra of *meso*-[{Ru(phen)$_2$}$_2$(μ-ppz)]$^{4+}$ bound to the dodecanucleotide [d(AT)$_6$]$_2$ were recorded at a range of temperatures. At a 1:1 ratio of metal complex-to-oligonucleotide a number of intermolecular NOEs were observed between metal complex protons on the metal complex and those of the dodecanucleotide. The H*b* and H*c* protons on the tail end of the ppz bridging ligand exhibited strong NOEs to sugar residue protons located towards the top of the minor groove of the oligonucleotide (specifically, the H4′/ H5′/H5″ protons), as well as NOEs of weaker intensity to H1′ and H2″ protons. *Ring d* phenanthroline protons exhibited a similar pattern of NOEs, whereas the H4′/ H5′/H5″ correlations of the *ring a* and *b* phen protons were only of medium intensity (see Figure 4.12). The strength and abundance of minor groove-based NOE signals is a strong indicator that this is the likely binding site of the metal complex; H2″

protons are formally located in the *major* groove, however they are accessible to ligands binding sufficiently deeply within the minor groove. These specific NOEs and the large upfield shifts of several phen *ring d* protons may hint at partial intercalation of the phen ligand, however this proves difficult to reconcile with the binding model described below.

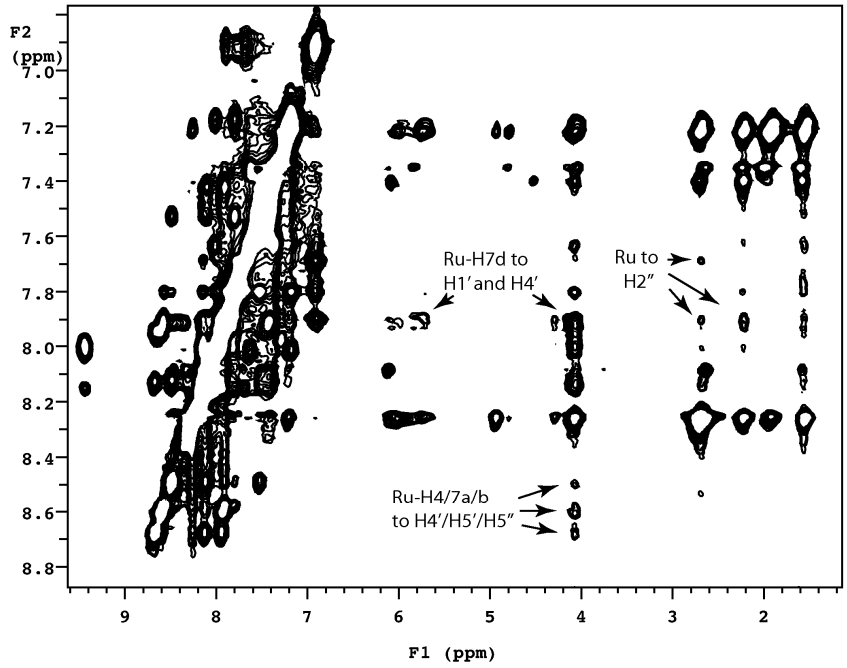

Figure 4.12
NOESY spectrum expansion of *meso*-[{Ru(phen)$_2$}$_2$(μ-ppz)]$^{4+}$ bound to the dodecanucleotide [d(AT)$_6$]$_2$. Spectrum obtained with a 300 ms mixing time at 25 °C, with a metal complex-to-dodecanucleotide ratio of 1.0. Labelled in the spectrum are several notable connectivities between metal complex terminal ligand protons and sugar residue protons of the oligonucleotide.

Once again, using NOE data as a guide it was possible to produce a simple molecular mechanics-based binding model of [d(AT)$_6$]$_2$ with added *meso*-[{Ru(phen)$_2$}$_2$(μ-ppz)]$^{4+}$ – in this instance using the MS Modeling 3.2[84] software package (and a HyperChem-generated dodecanucleotide model). As with the modelling of the hairpin-binding HAT-bridged complexes, the metal complex itself was treated as a rigid entity and the oligonucleotide energy-minimised around it. Minimisations, performed using CVFF, were undertaken from a variety of starting orientations in order to obtain the lowest energy model consistent with the observed NOE data. This model, depicted in Figure 4.13, has the ppz bridging ligand orientated *across* the minor groove in such a way as to bring its H*b* and H*c* protons into close proximity with the sugar phosphate backbone, consistent with the strong NOEs observed to the H4′/

H5′/H5″ sugar protons located toward the top of the minor groove. A slight inclination in the plane of the bridging ligand could potentially bring the H*c* ppz protons close enough to the minor groove H1′ protons to explain the weak NOE correlation observed between these resonances. Such an orientation also has *ring d* phen protons projecting deeper into the minor groove than any other, potentially explaining the large upfield shifts of these resonances and their medium-intensity NOE correlations to H2″ protons. The angle of these phen ligands relative to the inclination of the base pairs rules out the possibility of any intercalation. The other set of phen ligands – those possessing *ring a* and *b* protons – sit atop the ppz ligand, running parallel to the minor groove but projecting out into solution. Thus, the only conceivable NOEs likely to be observed for these protons would be to the minor groove protons on the extremities. While such correlations certainly are evident in the NOESY spectra, the intensity of the signals is hard to reconcile with the relatively large distances between the *ring a* and *b* phen protons and those of the minor groove in the model described here. Overall, this model resembles those of the hairpin-bound HAT complexes detailed above (with the bridging ligand lying *across* the minor groove), albeit with the opposite pair of phen ligands projecting into the groove (the *ring c*/*d* pair in the HAT complex, the *ring a*/*b* pair in the ppz complex). This observation is intriguing in that it contradicts the reasons postulated above for the greater affinity of the *meso* diastereoisomer; it is possible that the more flexible minor groove inherent in AT-rich sequences is able to more readily accommodate the less-ideally aligned ligands, and in doing so undergoes favourable non-covalent interactions that compensate for the resultant energy cost. Ultimately, the $[d(AT)_6]_2$–bound *meso*-$[\{Ru(phen)_2\}_2(\mu\text{-ppz})]^{4+}$ model presented here satisfies many of the observed NOE constraints, but not all; it may be that, given the broadness of the NMR resonances and the homogeneity of the binding sequence, there is an exchange between multiple binding states and that the NOESY spectra are representative of an average of these states, making it impossible to satisfy all NOE constraints with a single model.

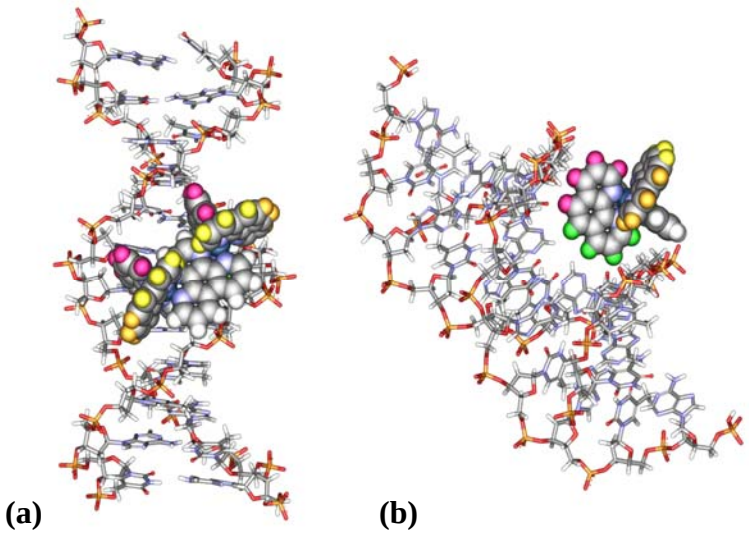

Figure 4.13
Model of *meso*-[{Ru(phen)$_2$}$_2$(μ-ppz)]$^{4+}$ bound to AT dodecanucleotide [d(AT)$_6$]$_2$. Energy minimised MS Modeling/CVFF model depicting a likely orientation of the metal complex as seen **(a)** looking down onto the plane of thee bridging ligand and **(b)** down the length of the minor groove. *Ring a* phenanthroline protons are depicted in orange, *ring b* in yellow, *ring c* in pink, and *ring d* in green.

4.3.7 Inhibition of Restriction Enzyme Activity at a TATA Box

The particular affinity of the complex *meso*-[{Ru(phen)$_2$}$_2$(μ-ppz)]$^{4+}$ for AT-rich DNA sequences, as demonstrated through FID assays (Chapter 3) and the NMR experiments described above, was further explored through the use of a restriction endonuclease inhibition assay. This complex exhibits a number of parallels to the TATA-box Binding Protein (TBP) in that it binds preferentially and with high affinity to the minor groove of an AT-rich DNA sequence. As a means by which to infer the utility of *meso*-[{Ru(phen)$_2$}$_2$(μ-ppz)]$^{4+}$ as a TBP binding inhibitor, restriction inhibition experiments were conducted using *Bst*Z17I, an enzyme that hydrolytically cleaves double-stranded DNA at the centre of the restriction site GTA↓TAC to produce blunt-ended fragments.

The 40-mer oligonucleotide d(GGC ACG TGG AAC TCT GGG **TAT A**CT CAG CGA GGC CTA CTC G)•d(CGA GTA GGC CTC GCT GAG **TAT A**CC CAG AGT TCC ACG TGC C), containing a central TATA box/*Bst*Z17I restriction site, was prepared by annealing equimolar portions of its constituent single strands. Samples of the oligonucleotide were titrated with aliquots of *meso*-[{Ru(phen)$_2$}$_2$(μ-ppz)]$^{4+}$ to varying concentrations, incubated with *Bst*Z17I for several hours and subjected to agarose gel electrophoresis. Digested

oligonucleotides (i.e. 20-mers) were expected to travel faster through the gel than were the undigested 40-mers; the degree to which digestion was successful could be extrapolated from the relative intensity of the ethidium bromide emission of the digested band when viewed under UV light. Initial attempts to assess inhibitive activity were unsuccessful because the metal complex itself interfered with the fluorescence of the DNA-bound ethidium bromide (this phenomenon being the original basis of the FID assay); this problem was overcome using an additional post-incubation step in which the metal complex was extracted using a small amount of SP Sephadex C-25 cation-exchange medium.

As shown in Figure 4.14, increasing concentrations of *meso*-$[\{Ru(phen)_2\}_2(\mu\text{-ppz})]^{4+}$ correlate to decreased restriction activity by the *Bst*Z17I enzyme: the intensity of the higher-mobility bands corresponding to the cleaved oligonucleotide vary inversely with the amount of metal complex. Such an observation might be explained by steric blockage and/or conformational deformation of the restriction site upon binding of the metal complex, thus interfering with the binding of the restriction enzyme. The reciprocal trend, an increase in the intensity uncleaved oligonucleotide bands with increasing metal complex concentration, is less obvious but still evident. The reason for this ambiguity is the presence of an impurity band of relatively low intensity that ran at the level of the undigested band. This impurity, believed to be an excess of one of the single strands from which the oligonucleotide was comprised, is evident even in digestions involving *no* metal complex (i.e. digestions in which *all* of the oligonucleotide should be converted to the cleaved form; see lane 2 of Figure 4.14, for instance).[†] While the quantity of *meso*-$[\{Ru(phen)_2\}_2(\mu\text{-ppz})]^{4+}$ needed to induced near-complete inhibition of endonucleolytic cleavage was quite high (200 μM, a complex-to-base pair ratio of 10:1), they were significantly smaller than those required by a high-affinity bisintercalating platinum complex and its inactive monointercalating analogue in similar experiments.[80]

[†] Attempts to digest the impurity with a vast excess of restriction enzyme and/or overnight digestion proved futile, demonstrating that it was not the target duplex.

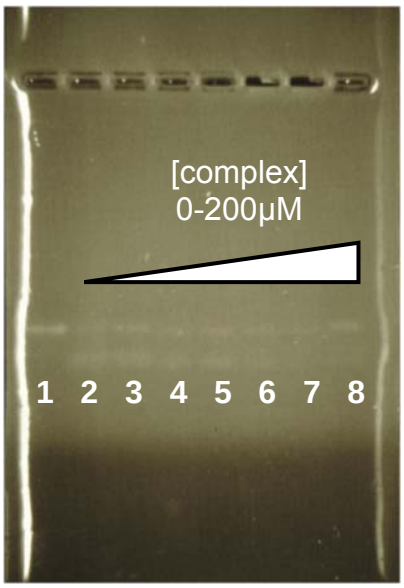

Figure 4.14
Image of an agarose gel depicting the inhibition of restriction enzyme *Bst*Z17I by *meso*-[{Ru(phen)$_2$}$_2$(μ-ppz)]$^{4+}$. Control lane 1 contains only the oligonucleotide, lanes 2-8 contain the oligonucleotide after being incubated with the restriction enzyme in the presence of increasing concentrations of the metal complex (lane 2: 0 μM, lane 3: 5 μM, lane 4: 10 μM, lane 5: 25 μM, lane 6: 50 μM, lane 7: 100 μM, lane 8: 200 μM). The lower, higher mobility band is due to the cleaved oligonucleotide, the upper band is the full-length oligonucleotide (or a single-stranded impurity – see text for details).

4.4 CONCLUSIONS & FUTURE DIRECTIONS

The NMR experiments detailed in this Chapter elucidate the structural basis of the interactions between inert dinuclear polypyridylruthenium(II) complexes and oligonucleotides. Specifically, the nature of the significant interaction between HAT-bridged complexes and hairpin-containing oligonucleotides was probed in further detail. The results of these experiments reaffirm the propensity of bulky dinuclear species of this type to target more open and/or flexible nucleic acid structures; in this instance the HAT-bridged complexes eschew canonical duplex DNA, and even the sequence containing single-base bulges to which bpm-bridged complexes bound so well, in favour of hairpin loop structures. One- and two-dimensional NMR evidence in the form of selective resonance broadening/shifting and NOE correlations advocate selective binding by the HAT-bridged complexes at the stem-loop interface of hairpin sequences, with a greater affinity for larger 6-base loops over the small 4-base loops. It would appear that the interface of the confined, duplex stem and the open, flexible loop provides the ideal compromise between accommodative capacity and energetically favourable intermolecular interactions.

With the particular affinity of HAT-bridged complexes for hairpin loops established, it remains to fine tune the selectivity of these interactions for loops of specific size and/or sequence. Such a goal will require systematic modifications to the nature and functionality of the terminal ligands of the metal complex, factors which evidently govern both affinity and selectivity. Hairpin loops are abundant in natural nucleic acids, typically as structural and/or protein-recognition features in RNA and often as aberrations in DNA. These stem-loop structures comprise a plethora of different sizes and sequences, often characteristic of the specific gene product or disorder with which they are associated. The capability to selectively target a particular hairpin would be an invaluable asset in the rational design of metallopharmaceuticals. As implied by the FID assays described in Chapter 3, there is a significant variation in apparent binding affinity between different loop sequences and, although this particular aspect was not investigated, one would expect variations to the stem sequence to have a similar effect. NMR experiments, although relatively time-consuming (and therefore not amenable to a high-throughput screening process), provide the most effective means by which to study the structural factors that govern these selectivities.

Despite the propensity of dinuclear polypyridylruthenium(II) complexes to selectively bind deviations in the canonical DNA double helix, one particular class of metal complex stood out in FID assays due to its unexpectedly strong interaction with an AT *duplex* sequence. The enhanced negative electrostatic potential of the minor groove in AT-rich sequences would conceivably make the dodecanucleotide $[d(AT)_6]_2$ the most inviting of the standard duplex sequences to cationic metal complexes – an assumption seemingly reflected in the FID assays. However, the ppz-bridged complexes (specifically, the variants with phen and Me_2phen as terminal ligands) bound to this oligonucleotide with an affinity equal-to or greater-than that for any of the non-duplex structures. NMR studies of the interaction between ΔΛ-$[\{Ru(phen)_2\}_2(\mu\text{-ppz})]^{4+}$ and $[d(AT)_6]_2$ confirm the strength of this association; the complex binds via deep insertion of phen moieties into the flexible minor groove. It is not immediately apparent from the NMR experiments why this metal complex would appear to bind more strongly than the analogous, almost structurally-identical HAT-bridged complex; feasibly, the additional aza-nitrogens of the HAT ligand may adversely affect the electronic properties of the complex with regards to binding affinity.

AT-rich DNA sequences are potentially important biological targets as they occur in a number of regulatory elements including TATA boxes. ΔΛ-$[\{Ru(phen)_2\}_2(\mu\text{-ppz})]^{4+}$ exhibited

some inhibitory activity towards a restriction enzyme that cleaves DNA in the middle of a TATA sequence. From this observation it can be inferred that the metal complex could also inhibit the binding of TBP to a TATA box; direct confirmation of this interference could be assessed using *transcription* inhibition assays. The selectivity of the inhibition remains to be established: it remains to be seen if the complex interferes significantly with other restriction enzymes that target subtly different DNA sequences. Nevertheless, the hairpin-binding HAT complexes and AT-binding ppz complexes demonstrate impressive affinity and selectivity that, through fine-tuning of their structure and functionality, might be exploited in the rational design of potent nucleic acid probes or metallopharmaceuticals.

4.5 REFERENCES

1. C. C. McDonald, W. D. Phillips and S. Penman, *Science*, **1964**, *144*, 1234-1237.
2. M. P. Schweizer, S. I. Chan and P. O. P. Ts'o, *J. Am. Chem. Soc.*, **1965**, *87*, 5241-5247.
3. C. C. McDonald, W. D. Phillips and J. Lazar, *J. Am. Chem. Soc.*, **1967**, *89*, 4166-4170.
4. P. O. P. Ts'o, N. S. Kondo, M. P. Schweizer and D. P. Hollis, *Biochemistry*, **1969**, *8*, 997-1029.
5. R. M. Scheek, R. Boelens, N. Russo, J. H. van Boom and R. Kaptein, *Biochemistry*, **1984**, *23*, 1371-1376.
6. D. Hare, L. Shapiro and D. J. Patel, *Biochemistry*, **1986**, *25*, 7456-7464.
7. D. J. Patel, L. Shapiro and H. D., *J. Biol. Chem.*, **1986**, *261*, 1223-1229.
8. J. Feigon, J. M. Wright, W. Leupin, W. A. Denny and D. R. Kearns, *J. Am. Chem. Soc.*, **1982**, *104*, 5540-5541.
9. J. Feigon, W. Leupin, W. A. Denny and D. A. Kearns, *Biochemistry*, **1983**, *22*, 5943-5951.
10. D. Frechet, D. M. Cheng, L.-S. Kan and P. O. P. Ts'o, *Biochemistry*, **1983**, *22*, 5194-5200.
11. D. R. Hare, D. E. Wemmer, S.-H. Chou and G. Drobny, *J. Mol. Biol.*, **1983**, *171*, 319-336.
12. M. A. Weiss, D. J. Patel, R. T. Sauer and M. Karplus, *Proc. Natl. Acad. Sci. USA*, **1984**, *81*, 130-134.
13. B. Furtig, C. Richter, J. Wohnert and H. Schwalbe, *ChemBioChem*, **2003**, *4*, 936-962.
14. J. D. Puglisi, R. Tan, B. J. Calnan, A. D. Frankel and J. R. Williamson, *Science*, **1992**, *257*, 76-80.
15. P. Z. Qin and T. Dieckmann, *Curr. Opin. Struct. Biol.*, **2004**, *14*, 350-359.
16. J. Ying and A. Bax, *J. Am. Chem. Soc.*, **2006**, *128*, 8372-8373.
17. F. A. Gollmick, M. Lorenz, U. Dornberger, J. von Langen, S. Diekmann and H. Fritzsche, *Nucleic Acids Res.*, **2002**, *30*, 2669-2677.
18. U. D. Pryyakumar and A. D. MacKerel Jr, *J. Am. Chem. Soc.*, **2005**, *128*, 678-679.
19. F. Aboul-ela, A. I. H. Murchie, S. W. Homans and D. M. J. Liley, *J. Mol. Biol.* , **1993**, *229*, 173-188.
20. M. J. J. Blommers, J. A. L. I. Walters, C. A. G. Haasnoot, J. M. A. Aelen, G. A. van der Marel, J. H. van Boom and C. W. Hilbers, *Biochemistry*, **1989**, *28*, 7491-7498.
21. F. J. M. van de Ven and C. W. Hilbers, *Eur. J. Biochem.*, **1988**, *178*, 1-38.
22. S. Neidle, *Nucleic Acid Structure and Recognition*, Oxford University Press, New York, NY, USA, **2002**.
23. D. J. Patel, *Biochemistry*, **1974**, *13*, 2396-2402.
24. X. Liu, H. Chen and D. J. Patel, *J. Biomol. NMR*, **1991**, *1*, 323-347.
25. X. Gao and D. J. Patel, *Biochemistry*, **1988**, *27*, 1744-1751.
26. D. E. Gilbert and J. Feigon, *Nucleic Acids Res.*, **1992**, *20*, 2411-2420.
27. G. G. Hu, X. Shui, F. Leng, W. Priebe, J. B. Chaires and L. D. Williams, *Biochemistry*, **1997**, *36*.
28. T. A. Early, D. A. Kearns, J. F. Burd, J. E. Larson and R. D. Wells, *Biochemistry*, **1977**, *16*, 541-551.
29. J. Feigon, W. A. Denny, W. Leupin and D. A. Kearns, *J. Med. Chem.*, **1984**, *27*, 450-465.
30. J. G. Pelton and D. E. Wemmer, *J. Am. Chem. Soc.*, **1990**, *112*, 1393-1399.

31. A. Fede, A. Labhardt, W. Bannwarth and W. Leupin, *Biochemistry*, **1991**, *30*, 11377-11388.
32. E. Trotta, E. D'Ambrosio, G. Ravagnan and M. Paci, *J. Biol. Chem.*, **1996**, *271*, 27608-27614.
33. W. H. Gmeiner, C. J. Hudalla, A. M. Soto and L. Marky, *FEBS Lett.*, **2000**, *465*, 148-152.
34. R. Cerdan, D. Payet, J.-C. Yang, A. A. Travers and D. Neuhaus, *Prot. Sci.*, **2001**, *10*, 504-518.
35. A. S. Brodsky and J. R. Williamson, *J. Mol. Biol.*, **1997**, *267*, 624-639.
36. M. H. Werner, J. R. Huth, A. M. Gronenborn and G. M. Clore, *Cell*, **1995**, *81*, 705-714.
37. S. D. Auweter, F. C. Oberstrass and F. H.-T. Allain, *J. Mol. Biol.*, **2007**, *367*, 174-186.
38. P. Wenter, L. Reymond, S. D. Auweter, F. H.-T. Allain and S. Pitsch, *Nucleic Acids Res.*, **2006**, *34*, e79.
39. C. R. Brodie, J. G. Collins and J. R. Aldrich-Wright, *Dalton Trans.*, **2004**, 1145-1152.
40. C. A. Franklin, J. V. Fry and J. G. Collins, *Inorg. Chem.*, **1996**, *35*, 7541-7545.
41. J. V. Fry and J. G. Collins, *Inorg. Chem.*, **1997**, *36*, 2919-2921.
42. M. Bacac, A. C. G. Hotze, K. van der Schilden, J. G. Haasnoot, S. Pacor, E. Alessio, G. Sava and J. Reedijk, *J. Inorg. Biochem.*, **2004**, *98*, 402-412.
43. N. J. Wheate, B. J. Evison, A. J. Herlt, D. R. Phillips and J. G. Collins, *Dalton Trans.*, **2003**, 3486-3492.
44. A. Gelasco and S. J. Lippard, *Biochemistry*, **1998**, *37*, 9230-9239.
45. T. A. Scahill, R. M. Jensen, D. H. Swenson, N. T. Hatzenbuhler, G. Petzold, W. Wierenga and N. D. Brahme, *Biochemistry*, **1990**, *29*, 2852-2860.
46. D. Norman, D. Live, M. Sastry, R. Lipman, B. E. Hingerty, M. Tomasz, S. Broyde and D. J. Patel, *Biochemistry*, **1990**, *29*, 2861-2875.
47. A. S. Thompson and L. H. Hurley, *J. Mol. Biol.*, **1995**, *252*, 86-101.
48. M. Sastry, R. Fiala, R. Lipman, M. Tomasz and D. J. Patel, *J. Mol. Biol.*, **1995**, *247*, 338-359.
49. S. S. David and J. K. Barton, *J. Am. Chem. Soc.*, **1993**, *115*, 2984-2985.
50. R. Caspar, L. Musatkina, A. Tatosyan, H. Amouri, M. Gruselle, C. Guyard-Duhayon, R. Duval and C. Cordier, *Inorg. Chem.*, **2004**, *43*, 7986-7993.
51. J. G. Collins, A. D. Sleeman, J. R. Aldrich-Wright, I. Greguric and T. W. Hambley, *Inorg. Chem.*, **1998**, *37*, 3133-3141.
52. J. G. Collins, J. R. Aldrich-Wright, I. D. Greguric and P. A. Pellegrini, *Inorg. Chem.*, **1999**, *38*, 5502-5509.
53. I. Greguric, J. R. Aldrich-Wright and J. G. Collins, *J. Am. Chem. Soc.*, **1997**, *119*, 3621-3622.
54. J. P. Rehmann and J. K. Barton, *Biochemistry*, **1990**, *29*, 1701-1709.
55. J. P. Rehmann and J. K. Barton, *Biochemistry*, **1990**, *29*, 1710-1717.
56. M. Eriksson, M. Leijon, C. Hiort, B. Norden and A. Graslund, *Biochemistry*, **1994**, *33*, 5031-5040.
57. M. Eriksson, M. Leijon, C. Hiort, B. Nordén and A. Gräslund, *J. Am. Chem. Soc.*, **1992**, *114*, 4933-4934.
58. C. M. Dupureur and J. K. Barton, *J. Am. Chem. Soc.*, **1994**, *116*, 10286-10287.
59. C. M. Dupureur and J. K. Barton, *Inorg. Chem.*, **1997**, *36*, 33-43.
60. F. M. Foley, F. R. Keene and J. G. Collins, *J. Chem. Soc., Dalton Trans.*, **2001**, 2968-2974.

61. F. M. Foley, *DNA Interactions of Mono- and Dinuclear Polypyridylruthenium(II) Complexes*, Honours Thesis, James Cook University, Townsville, **2000**.
62. A. Kirsch-De Mesmaeker, C. Moucheron and N. Boutonnet, *J. Phys. Org. Chem.*, **1998**, *11*, 566-576.
63. O. van Gijte and A. Kirsch-De Mesmaeker, *J. Chem. Soc., Dalton Trans.*, **1999**, 951-956.
64. A. Brodkorb, A. Kirsch-De Mesmaeker, T. J. Rutherford and F. R. Keene, *Eur. J. Inorg. Chem.*, **2001**, 2151-2160.
65. B. T. Patterson, J. G. Collins, F. M. Foley and F. R. Keene, *J. Chem. Soc., Dalton Trans.*, **2002**, 4343-4350.
66. J. A. Smith, J. G. Collins, B. T. Patterson and F. R. Keene, *Dalton Trans.*, **2004**, 1277-1283.
67. J. A. Smith, *Dinuclear Ruthenium Complexes as Sequence- and Structure-Selective Binding Agents for DNA*, Honours Thesis, James Cook University, Townsville, **2003**.
68. B. T. Patterson, *Stereochemistry and Applications of Mono- and Oligo-nuclear Complexes of Iron, Ruthenium and Osmium*, PhD Thesis, James Cook University, Townsville, **2002**.
69. P. U. Maheswari, V. Rajendiran, M. Palaniandavar, R. Parthasarathi and V. Subramanian, *J. Inorg. Biochem.*, **2006**, *100*, 3-17.
70. P. U. Maheswari and M. Palaniandavar, *Inorg. Chim. Acta*, **2004**, *357*, 901-912.
71. C. B. Spillane, J. A. Smith, D. P. Buck, J. G. Collins and F. R. Keene, *Dalton Trans.*, **2007**, 5290-5296.
72. J. L. Morgan, D. P. Buck, A. G. Turley, J. G. Collins and F. R. Keene, *Inorg. Chim. Acta*, **2006**, *359*, 888-898.
73. J. L. Morgan, C. B. Spillane, J. A. Smith, D. P. Buck, J. G. Collins and F. R. Keene, *Dalton Trans.*, **2007**, 4333-4342.
74. J. L. Morgan, D. P. Buck, A. G. Turley, J. G. Collins and F. R. Keene, *J. Biol. Inorg. Chem.*, **2006**, *11*, 824-834.
75. Y. Kim, G. J. H., S. Hahn and P. B. Sigler, *Nature*, **1993**, *365*, 512-520.
76. J. L. Kim, D. B. Nikolov and S. K. Burley, *Nature*, **1993**, *365*, 520-527.
77. D. K. Lee, M. Horikoshi and R. G. Roeder, *Cell*, **1991**, *67*, 1241-1250.
78. D. B. Starr and D. K. Hawley, *Cell*, **1991**, *67*, 1231-1240.
79. Z. S. Juo, T. K. Chiu, P. M. Leiberman, I. Baikalov, A. J. Berk and R. E. Dickerson, *J. Mol. Biol.*, **1996**, *261*, 239-254.
80. J. R. Choudhury and U. Bierbach, *Nucleic Acids Res.*, **2005**, *33*, 5622-5632.
81. D. J. States, R. A. Haberkorn and D. J. Ruben, *J. Magn. Reson.*, **1982**, *48*, 286-292.
82. J. Sambrook, E. F. Fritsch and T. Maniatis, *Molecular Cloning: A Laboratory Manual*, Cold Spring Harbour Press, Cold Spring Harbour, NY, USA, **1989**.
83. *HyperChem 7.5*, HyperCube, Inc., Gainsville, FL, USA, **2005**.
84. *MS Modeling 3.2*, Accelrys Software, Inc., San Diego, CA, USA, **2005**.
85. W. D. Cornell, P. Cieplak, C. I. Bayly, I. R. Gould, K. M. Merz Jr., D. M. Ferguson, D. C. Spellmeyer, T. Fox, J. W. Caldwell and P. A. Kollman, *J. Am. Chem. Soc.*, **1995**, *117*, 5179-5197.
86. M. C. Zerner, *Semiempirical Molecular Orbital Methods*, in *Reviews in Computational Chemistry II*, eds. K. B. Lipkowitz and D. B. Boyd, Wiley, New York, NY, USA, **1991**.
87. A. K. Rappé, C. J. Casewit, K. S. Colwell, W. A. Goddard III and W. M. Skiff, *J. Am. Chem. Soc.*, **1992**, *114*, 10024-10035.

88. A. K. Rappé, K. S. Colwell and C. J. Casewit, *Inorg. Chem.*, **1993**, *32*, 3438-3450.
89. P. Dauber-Osguthorpe, V. A. Roberts, D. J. Osguthorpe, J. Wolff, M. Genest and A. T. Hagler, *Protein. Struct. Funct. Genet.*, **1988**, *4*, 31-47.
90. T. C. Jenkins, *Evaluation of Drug-Nucleic Acid Interactions by Thermal Melting Curves*, in *Drug-DNA Interaction Protocols*, ed. K. Fox, Humana Press, Totowa, NJ, USA, **1997**, pp. 195-218.
91. M. W. Kalnik, D. G. Norman, P. F. Swann and D. J. Patel, *J. Biol. Chem.*, **1989**, *264*, 3702-3712.
92. P. T. Henderson, B. Armitage and G. B. Schuster, *Biochemistry*, **1998**, *37*, 2991-3000.
93. D. J. Patel, L. Shapiro and D. Hare, *J. Biol. Chem.*, **1986**, *261*, 1223-1229.
94. J. G. Collins, *Biochem. Int.*, **1988**, *16*, 819-828.
95. P. N. Borer, Y. Lin, S. Wang, M. W. Roggenbuck, J. M. Gott, O. C. Uhlenbeck and I. Pelczer, *Biochemistry*, **1995**, *34*, 6488-6503.
96. L. Varani, M. Hasegawa, M. G. Spillantini, M. J. Smith, J. R. Murrell, B. Ghetti, A. Klug, M. Goedert and G. Varani, *Proc. Natl. Acad. Sci. USA*, **1999**, *96*, 8229-8234.
97. D. R. Davies and R. L. Baldwin, *J. Mol. Biol.*, **1963**, *6*, 251-256.
98. D. A. Marvin, M. Spencer, M. H. F. Wilkins and L. D. Hamilton, *J. Mol. Biol.*, **1961**, *3*, 547-565.
99. H. R. Drew and R. E. Dickerson, *EMBO J.*, **1982**, *1*, 663-667.
100. G. Gupta, M. H. Sarma, M. M. Dhingra, R. H. Sarma, M. Rajagopalan and V. Sasisekharan, *J. Biol. Struct. Dyn.*, **1983**, *1*, 395-416.
101. N. G. A. Abrescia, C. Gonzlez, C. Gouyette and J. A. Subirana, *Biochemistry*, **2004**, *43*, 4092-4100.
102. J. L. Campos, L. Urpi, a. San, T. , C. Gouyette and J. A. Subirana, *Proc. Natl. Acad. Sci. USA*, **2005**, *102*, 3663-3666.
103. E. T. Zuo, F. A. Tanious, W. D. Zilson, G. Zon, G.-S. Tan and R. M. Wartell, *Biochemistry*, **1990**, *29*, 4446-4456.
104. S. Arnott and D. W. L. Hukins, *Biochem. Biophys. Res. Comm*, **1972**, *47*, 1504-1509.
105. U. Schmitz, d. A. Pearlman and T. L. James, *J. Mol. Biol.*, **1991**, *221*, 271-292.
106. A. G. W. Leslie and S. Arnott, *J. Mol. Biol.*, **1980**, *143*, 49-72.
107. M. A. Viswamitra, Z. Shakked, P. G. Jones, G. M. Sheldrick, S. A. Salisbury and O. Kennard, *Biopolymers*, **1982**, *21*, 513-533.
108. N. Assa-Munt and D. R. Kearns, *Biochemistry*, **1984**, *23*, 791-796.
109. A. Klug, A. Jack, M. A. Viswamitra, O. Kennard, Z. Shakked and T. A. Steitz, *J. Mol. Biol.*, **1979**, *131*, 669-680.
110. B. Borah, J. S. Cohen and A. Bax, *Biopolymers*, **1984**, *24*, 747-765.
111. J. Kypr, J. Chládková, L. Arnold, J. Sági, A. Szemzö and M. Vorlícková, *J. Biomol. Struct. Dyn.*, **1996**, *13*, 999-1006.
112. S. Arnott and E. Selsing, *J. Mol. Biol*, **1974**, *88*, 509-521.
113. S. Arnott, R. Chandrasekaran, L. C. Puigjaner, J. K. Walker, I. H. JHall and D. L. Birdsall, *Nucleic Acids Res.*, **1983**, *11*, 1457-1474.
114. N. Zhou, A. M. Bianucci, N. Pattabiraman and T. L. James, *Biochemistry*, **1987**, *26*, 7905-7913.
115. E.-I. Suzuki, N. Pattabiraman, G. Zon and T. L. James, *Biochemistry*, **1986**, *25*, 6854-6865.
116. C. B. Spillane, J. L. Morgan, N. C. Fletcher, J. G. Collins and F. R. Keene, *Dalton Trans.*, **2006**, 3122-3133.

117. J. R. Aldrich-Wright, I. D. Greguric, C. H. Y. Lau, P. Pellegrini and J. G. Collins, *Recent Res. Devel. in Inorganic Chem.*, **1998**, *1*, 13-35.
118. J. G. Collins, R. M. Rixon and J. R. Aldrich-Wright, *Inorg. Chem.*, **2000**, *39*, 4377-4379.

Chapter 5

Separation of Metal Complex Stereoisomers Using DNA-Affinity Chromatography

5.1 INTRODUCTION

5.1.1 Affinity Chromatography

Affinity chromatography is broadly defined as a chromatographic technique for separating an analyte from a biochemical mixture on the basis of "biological affinity".[1-4] The specificity of the biological interactions being exploited typically arise from a variety of non-covalent associations – electrostatic, hydrogen bonding, hydrophobic, van der Waals, and chiral/steric complementarity – between a receptor and a ligand.[† 5] Typically, one constituent of the interacting system, the *affinity ligand*, is immobilised on an insoluble porous support and packed into a column. When a mixture of biomolecules is passed down the column, specific components are selectively adsorbed and their passage retarded. Those molecules without a substantial affinity for the ligand wash through the column with little impediment, thus resulting in the purification and isolation of the analyte. The adsorbed species may subsequently be eluted from the column by altering the conditions of the eluent through variation in ionic strength or pH, or by introducing a competitive binding target to the solution.

This technique has been in routine use for over forty years within disciplines ranging from molecular biology through to the pharmaceutical sciences and biotechnology, and it is finding increasing applications in clinical diagnoses. Most commonly, affinity chromatography is employed in the purification antibodies and antigens,[6, 7] oligosaccharides and glycoproteins,[8, 9] hormones,[10, 11] and enzymes.[12, 13] Using the latter case as an example, enzymes are commonly purified by means of an immobilised inhibitor of the specific enzyme to be isolated. Trypsin, for instance, can be purified using chicken ovomucoid (an egg white protein found to inhibit trypsin) as the affinity ligand.[14, 15] While affinity ligands have historically been biological molecules (or derivatives thereof) themselves, rationally-designed non-biological and biomimetic adsorbents have become the focus or more recent advances in the technique.[3, 16-18]

5.1.2 DNA as a Chromatographic Medium

While specific classes of protein or peptide most commonly play the role of the affinity ligand in affinity chromatography, polynucleotides have also been successfully employed in

[†] In this instance "ligand" is the biological usage of the word: an ion or molecule that binds to specific biomolecules in order to form a larger complex with a biological purpose.

this capacity for the purification and isolation of nucleic acid-binding biomolecules.[19, 20] This specific application of affinity chromatography was first reported by Litman in 1968 for the purification of DNA polymerase,[21] but has since been applied to numerous other DNA-binding proteins such as transcription factors,[20, 22, 23] telomerases,[24] or nucleases,[25] as well as the purification of other nucleic acids via complimentary DNA-DNA and DNA-RNA interactions.[26, 27]

Biochemical separations utilising nucleic acids as the affinity ligand have typically operated primarily on the basis of sequence selectivity rather than exploiting potential chiral complementarity in the resolution of enantiomeric mixtures. Affinity-based chiral separations have largely been confined to HPLC-type experiments in which proteins or carbohydrates have been employed in the role of affinity ligand,[4, 28-30] often for the resolution of drug enantiomers. For example, α_1-acid glycoprotein has been used to resolve the *R*-(+)- and *S*-(-)- isomers of the anaesthetic agent thiopentone,[31] while *β*-cyclodextrin columns have facilitated the separation of (*S*)-propranolol, a drug used for the treatment of hypertension, from its less active (*R*)-counterpart.[32]

A field in which the chiral-resolving capabilities of DNA have received some attention relates to the resolution of metal complex enantiomers on the basis of enantioselectivities observed in general DNA-binding studies. Baker *et al*. have reported the enantiomeric resolution of racemic mixtures of the complexes $[Ru(phen)_3]^{2+}$ and $[Ru(bpy)_2(ppz)]^{2+}$ by means of elution through a DNA-hydroxylapatite column.[33] In each instance, the Λ isomer was found to elute prior to the Δ isomer, consistent with the stronger DNA-binding affinity observed for the latter form.[34-36] Similar mononuclear DNA-intercalating complexes have been resolved by Aldrich-Wright and co-workers using a HPLC technique employing a covalently-bound DNA stationary phase.[37] Complex retention was found to be related to pH and ligand size. Capillary electrophoresis-facilitated resolutions of racemic mixtures of $[Ru(bpy)_3]^{2+}$ and $[Ru(phen)_3]^{2+}$ have also been achieved using calf thymus DNA as a chiral medium.[38] Aldrich-Wright was also involved in the development of a technique in which DNA-impregnated cellulose paper was used to compare retention times of DNA-binding complexes and relate them to the intercalative ability of various ligands.[39] A similar DNA/paper chromatographic technique was reported by Hannon *et al.* to resolve the enantiomeric forms of metallo-supramolecular triple-helicates (although the DNA-free cellulose alone was itself quite efficient at resolving the enantiomers).[40] Chiral separations of transition metal complexes have also been accomplished

using capillary electrophoresis with a selection of chiral buffer additives, including calf-thymus DNA.[41]

5.1.3 Present Studies

While the cation-exchange chromatographic techniques described in Chapter 2 have proven very effective in the isolation of stereochemically-pure dinuclear polypyridylruthenium(II) complexes, there are some systems – particularly those with flexible bridging ligands – for which enantiomeric resolution remains elusive. Given that the purpose of acquiring such stereochemically-pure complexes was often to study their stereoselective interactions with nucleic acids, it was considered that DNA-based chromatographic method might yield more efficient resolutions while at the same time providing a general indication of relative DNA-binding affinities. Towards this end, a new column-based affinity chromatography technique was developed for the separation of stereoisomeric metal complexes containing polypyridyl ligands. Specifically, the technique was intended to exploit the particular affinity of dinuclear polypyridylruthenium(II) complexes for *non-duplex* nucleic acids in affecting highly-efficient diastereoisomeric separations and enantiomeric resolutions.

5.2 EXPERIMENTAL

5.2.1 Materials

HiTrap Streptavidin HP pre-packed columns, Streptavidin Sepharose High Performance media, and a Tricorn 10/150 empty high-performance glass column were purchased from GE Healthcare (formerly Amersham Biosciences). Sodium phosphate (Na_3PO_4; Aldrich, 96%), sodium chloride (NaCl, Ajax) and ethanol (95%, APS Ajax) were used as supplied. Biotinylated oligonucleotides were obtained from GeneWorks. All solutions were filtered through a 0.45 μM Millex HA syringe filter before being chromatographed.

5.2.2 Physical Measurements

Electronic absorption spectra were recorded in aqueous buffer solution on a Cary 5E spectrophotometer and circular dichroism spectra were recorded on a Jasco J-715

spectropolarimeter. Spectra were obtained in phosphate buffer solutions (see below for specific concentrations) containing metal complex concentrations in the low micromolar range.

5.2.3 Synthesis of Metal Complexes

Dinuclear metal complexes were prepared as described in Chapter 2 and converted to the water-soluble chloride salts as described in Chapter 3. $[Ru(phen)_3]Cl_2$ {phen = 1,10-phenanthroline) was prepared using a similar method to that described in Chapter 2: $RuCl_3.3H_2O$ (Strem; 50 mg) and phen (Aldrich, 99+%; 160 mg) were refluxed together in a microwave oven on "medium-high" for 2 minutes. The resultant orange solution was subjected to cation-exchange chromatography and the PF_6 salt isolated in 96% yield (170 mg). The complex was subsequently purified on a silica gel column and methathesised to the chloride salt using an anion-exchange resin. $[Ru(4\text{-}Mebpy)_3]Cl_2$, provided by Dr. Caitriona Spillane (from the Keene laboratory), was prepared using a similar technique. $[\{Ru(phen)_2\}_2(\mu\text{-dppm})]^{4+}$ and $[\{Ru(phen)_2\}_2(\mu\text{-bb7})]^{4+}$ were prepared by Dr. Joy Morgan (from the Keene laboratory) using reported methods.[42, 43] $[Ru_2(qtpy)_3]^{4+}$ {qtpy = 5,5‴-dimethyl-2,2′:5′,5″:2″,2‴-quaterpyridine} was supplied by Mr. Chris Glasson (Meehan laboratory, JCU).

5.2.4 Chromatography

These chromatographic experiments were performed on two scales: a small scale using columns pre-packed with a medium of streptavidin immobilised on Sepharose and a larger scale using the same medium in bulk. In the former, a pre-packed HiTrap Streptavidin HP column (0.7 × 2.5 cm, 1 mL) was attached to a Gilson Minipuls 3 peristaltic pump and equilibrated with approximately ten volumes (10 mL) of a pH 7.5 of a sodium phosphate buffer solution at a rate of 1 mL min^{-1} (see below for concentrations). Approximately 300 nmol of a biotinylated oligonucleotide was then loaded on the column in the same buffer solution (1-2 mL) at a rate of 0.1-0.5 mL min^{-1}, and the column was subsequently washed additional buffer (10 mL at 1 mL min^{-1}). The nucleic acid was adsorbed to the Streptavidin Sepharose support through the exceptionally strong biotin-streptavidin non-covalent bond (see Figure 5.1), an association routinely exploited in numerous biotechnology-related applications, including affinity-based chromatographic techniques.[44-46] Periodic measurements of the absorbance of the column wash

were made at 260 nm to ensure no DNA was being eluted; if DNA was present, the wash was recycled onto the column until it was DNA-free or the column saturated.

Once the DNA was adequately immobilised the desired metal complex mixture (100 nmol in *ca.* 500 μL of buffer solution) was loaded on the column and eluted once again with sodium phosphate buffer solution containing sodium chloride. The concentration of the buffer solution varied depending on the resolution required; higher concentrations (i.e. 20 mM phosphate buffer/0.15M chloride) facilitated the separation of different complexes, intermediate concentrations (10 mM phosphate buffer/0.075 M chloride) allowed for the separation of diastereoisomers and most enantiomers, while relatively low concentrations (5 mM phosphate buffer/0.0375 M chloride) were required for some more difficult resolutions. Elution times and volumes varied depending on the concentration of the eluent and the natures of both the oligonucleotides and complexes being used. Nevertheless, separations of complexes, diastereoisomers and enantiomers could be clearly observed on the white columns due to the highly coloured nature of the complexes. The identity of the eluted species were confirmed by examination of the UV/Vis and circular dichroism (CD) spectra of the eluate solutions.

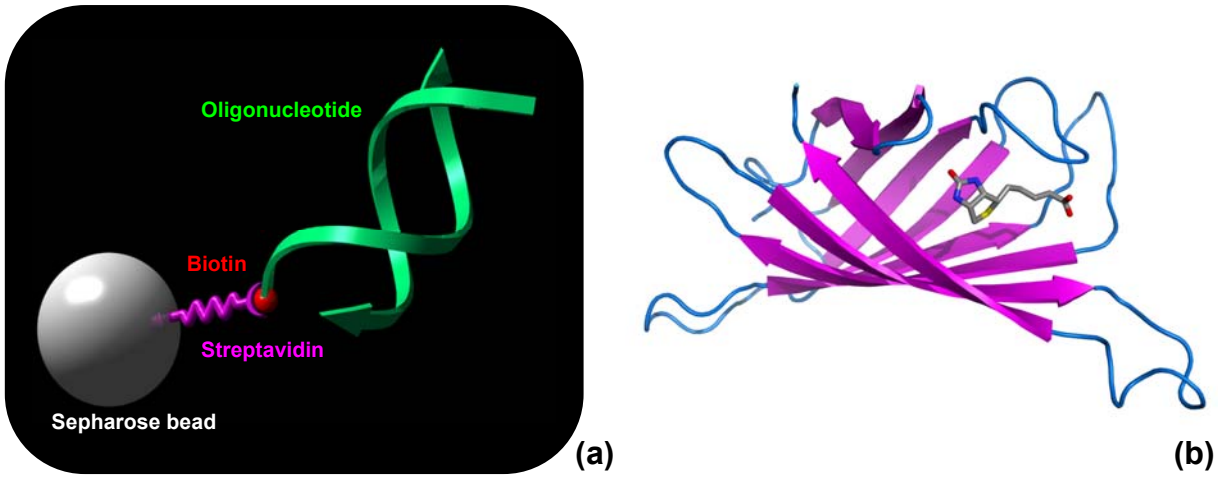

Figure 5.1
The streptavidin-biotin bond. (a) A schematic representation of the affinity chromatography medium. Streptavidin, covalently bound to Sepharose beads, binds non-covalently to biotin covalently attached to a synthetic oligonucleotide. (b) X-ray crystal structure (PDB structure **2izh**, rendered with PyMOL)[47] of the monomeric unit of the tetrameric streptavidin protein isolated from the bacterium *Streptomyces avidinii*. The protein is represented in ribbon form while the bound vitamin biotin is represented in stick form.

In the scaled-up methodology, a Tricorn 10/150 column (10 mm × 150 mm, volume *ca.* 10 mL with adapters attached) was filled with a slurry of Streptavidin Sepharose HP in 20% ethanol and left to settle for several hours. The column was connected to a peristaltic pump and

approximately ten volumes (100 mL) of sodium phosphate/sodium chloride buffer solution passed through the column at a rate of *ca.* 1 mL min^{-1} to equilibrate the medium (again, the concentration of the buffer solution was dependent upon the nature of the species being separated). The column was subsequently charged with *ca*. 2.4 µmol of biotinylated bulge oligonucleotide {d(CCG**A**GAATTCCGG)$_2$} and the wash solution recycled through the medium to ensure maximum DNA binding. After further washing with more buffer solution the column was loaded with the mixture of interest; the scaled-up methodology was found capable of handling 1-2 µmol (*ca.* 2 mg) of complex in most instances (slightly larger amounts of more readily separated complexes could be accommodated). Eluted material was again identified using UV/Vis and CD spectroscopies.

The relative sizes of the original and scaled-up apparatus are illustrated in Figure 5.2. Both the bulk Sepharose medium and the HiTrap columns were stored in 20% ethanol solution in a refrigerator between uses.

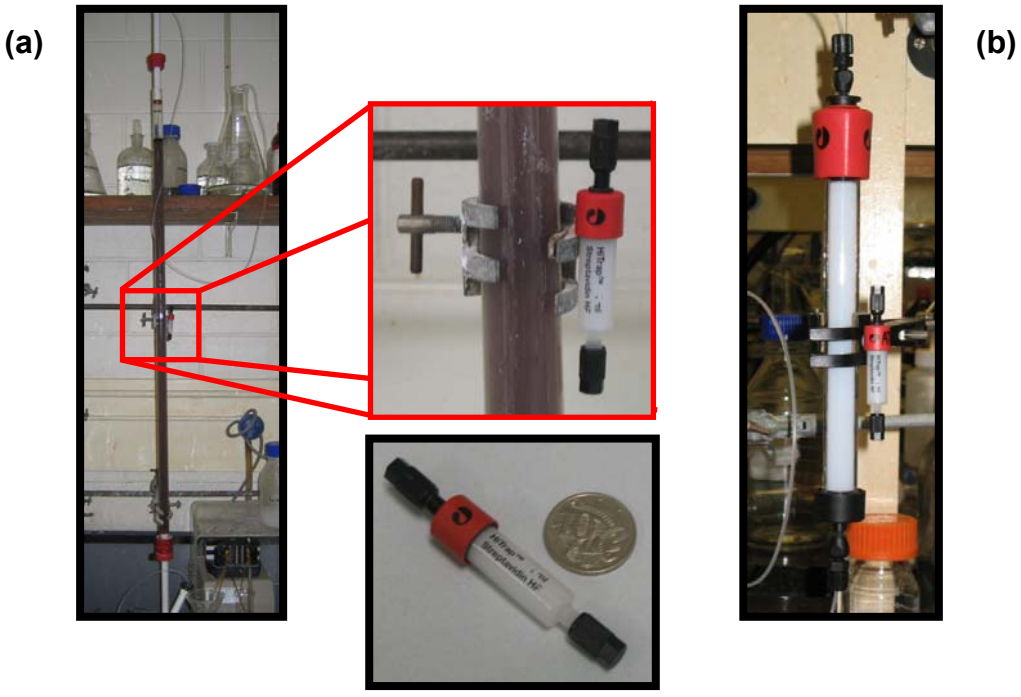

Figure 5.2
DNA-affinity chromatography columns. Side-by-side comparisons of the HiTrap affinity chromatography column with (a) the column used for a typical cation-exchange chromatography experiment and (b) the scaled-up affinity chromatography apparatus alongside the smaller HiTrap column.

5.3 RESULTS & DISCUSSION

5.3.1 Separation of Different Complexes

The first test of this method involved the separation of the equivalent diastereoisomer of two different complexes – *meso*-[{Ru(Me_2bpy)$_2$}$_2$(μ-bpm)]$^{4+}$ and *meso*-[{Ru(phen)$_2$}$_2$(μ-HAT)]$^{4+}$ – on an immobilised tridecanucleotide possessing an unpaired adenine base (or "bulge"), d(CCG**A**GAATTCCGG)$_2$. This particular oligonucleotide was selected because it had been used in several prior DNA-binding studies by our group.[48-50] A relatively concentrated eluent was used for this first separation (20 mM sodium phosphate buffer/0.15 M sodium chloride) and a clear separation of the two complexes was observed over the 2.5 cm length of the column. Collection of a green band corresponding to the bpm-bridged complex took place after 3-8 mL of eluent had passed through the column, while the trailing purple band of the HAT-bridged species was collected after the passage of 130-200 mL of eluent. The elution order of these two complexes reflects the relative binding affinities of the two complexes with this particular oligonucleotide as observed in fluorescent intercalator displacement (FID) asays (see Chapter 3): *meso*-[{Ru(Me_2bpy)$_2$}$_2$(μ-bpm)]$^{4+}$ was found to decrease the fluorescence of d(CCG**A**GAATTCCGG)2-bound ethidium bromide (EthBr) by some 33%, while *meso*-[{Ru(phen)$_2$}$_2$(μ-HAT)]$^{4+}$ induced a 62% decrease (see Figure 5.3).

This procedure was repeated on a column to which an icosamer featuring a 6-base CT hairpin loop, d(CACTGGT**CTCTCT**ACCAGTG), had been immobilised. Again, a clear separation of the green and purple bands was observed with the same elution order, in concordance with binding affinities suggested by the FID assay (Figure 5.3).

In order to ascertain that it was indeed the DNA (rather than the Streptavidin Sepharose support) that was responsible for the separation the same mixture of complexes was loaded on a column to which no DNA had been bound. No separation was observed, confirming the influence of the oligonucleotides.

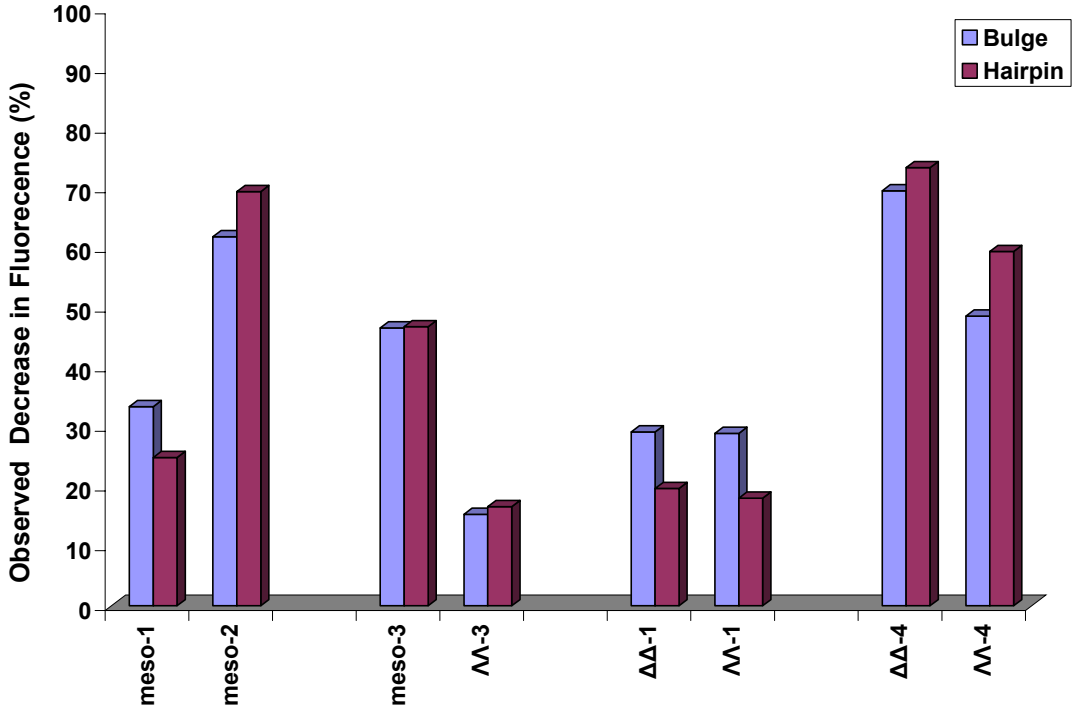

Figure 5.3
FID assay data pertaining to the oligonucleotide-complex interactions investigated by DNA-affinity chromatography. Bulge = d(CCG**A**GAATTCCGG)$_2$; Hairpin = d(CACTGGT**CTCTCT**ACCAGTG); **1** – [{Ru(Me$_2$bpy)$_2$}$_2$(μ-bpm)]$^{4+}$; **2** – [{Ru(phen)$_2$}$_2$(μ-HAT)]$^{4+}$; **3** – [{Ru(bpy)$_2$}$_2$(μ-HAT)]$^{4+}$; **4** – [{Ru(phen)$_2$}$_2$(μ-2,3-dpp)]$^{4+}$. Larger decreases in fluorescence are taken to represent a higher binding affinity. For further details on the FID method refer to Chapter 3.

5.3.2 Separation of Diastereoisomers

The second system examined by this technique was a diastereoisomeric mixture (*meso* and ΛΛ) of the complex [{Ru(bpy)$_2$}$_2$(μ-HAT)]$^{4+}$ {bpy = 2,2′-bipyridine}. Using a column containing the immobilised bulge sequence with an eluent of half the previous concentration (i.e. 10 mM sodium phosphate buffer/0.075 M sodium chloride), a clear separation of two purple bands was achieved. The first band was collected after 25-30 mL of eluate, the second after 35-50 mL. CD spectra revealed that the first band was the ΛΛ isomer, while the second band was the *meso* isomer (see Figure 5.4). The greater apparent affinity of the *meso* diastereoisomer for the bulge sequence is in agreement with FID assay results that showed a 47% decrease in EthBr fluorescence upon the addition of *meso*-[{Ru(bpy)$_2$}$_2$(μ-HAT)]$^{4+}$ compared to a decrease of only 15% upon the addition of the ΛΛ isomer (see Figure 5.3).

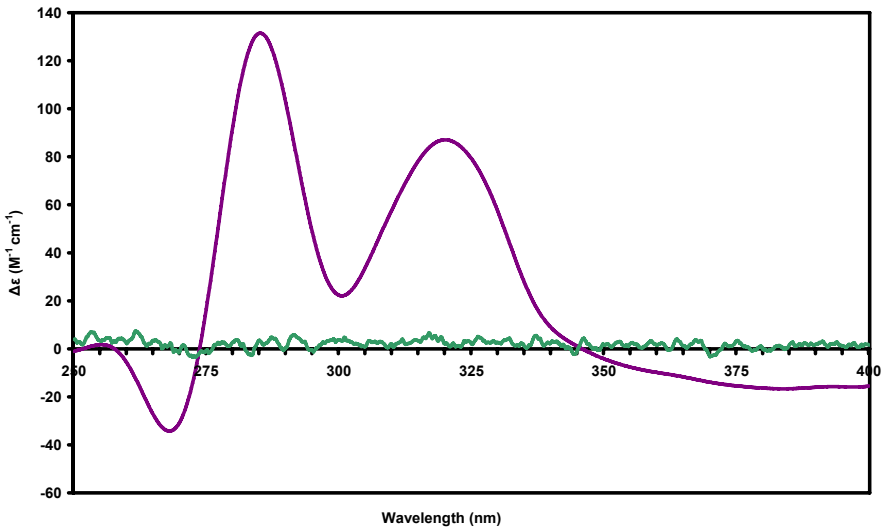

Figure 5.4
Separation of diastereoisomers using non-duplex DNA. The CD spectra of the first (violet) and second (green) bands eluted from a mixture of ΛΛ- and *meso*-$[\{Ru(bpy)_2\}_2(\mu\text{-HAT})]^{4+}$ separated on a HiTrap column loaded with the bulge-containing oligonucleotide d(CCG**A**GAATTCCGG)2. The first band corresponds to the ΛΛ enantiomer, the second to the *meso* diastereoisomer.

5.3.3 Resolution of Enantiomers

The next logical step in the testing of the technique was an attempt to resolve a racemic mixture of $[\{Ru(Me_2bpy)_2\}_2(\mu\text{-bpm})]^{4+}$. As explained in Chapter 3, this system proved to be a failure of the original EthBr FID assay as both the ΔΔ and ΛΛ enantiomers induced a fluorescence decrease of 29% upon binding to the bulge-containing oligonucleotide $d(CCG\mathbf{A}GAAATTCCGG)_2$. This is in contrast to NMR experiments on the interaction of these enantiomers with the same oligonucleotide that demonstrated total enantioselectivity for the bulge site.[49] Nevertheless, resolution of this racemic mixture was accomplished on a HiTrap column with an eluent solution of 10 mM sodium phosphate buffer and 0.075 M sodium chloride. Two green bands eluted from the column with CD spectra identifying the first as the ΛΛ isomer and the second as the ΔΔ isomer (see Figure 5.5). Although the ease of separation observed here does not concur with the results of the original EthBr FID assay, it does reflect the results of NMR experiments and the modified FID technique utilising DAPI (4',6-diamidino-2-phenylindole; see below and Chapter 3 for further details).

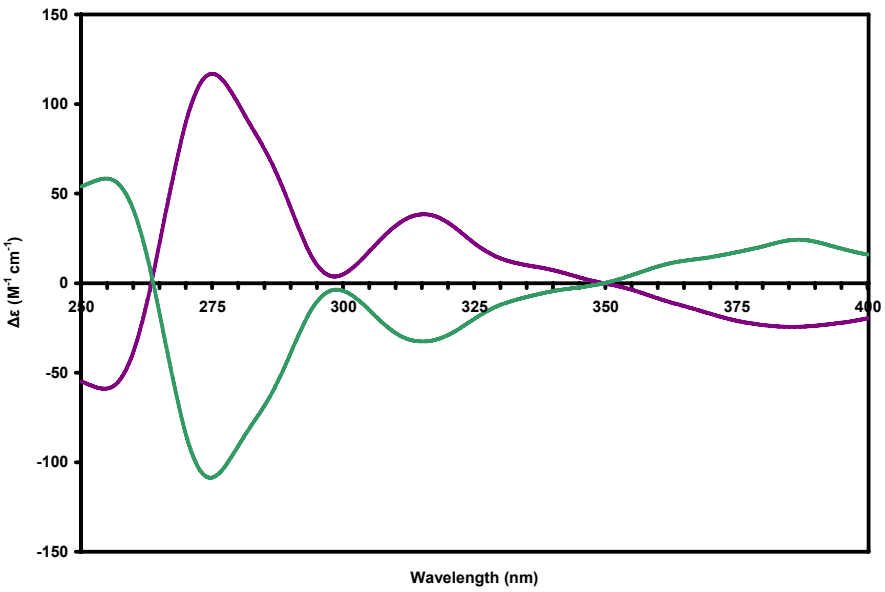

Figure 5.5
Resolution of enantiomers using non-duplex DNA. The CD spectra of the first (violet) and second (green) bands eluted from a mixture of ΔΔ- and ΛΛ-$[\{Ru(Me_2bpy)_2\}_2(\mu\text{-bpm})]^{4+}$ separated on a HiTrap column loaded with the bulge-containing oligonucleotide d(CCG**A**GAATTCCGG)$_2$. The first band corresponds to the ΛΛ enantiomer, the second to the ΔΔ enantiomer.

Having successfully applied the DNA-affinity technique to one of the racemic mixtures most readily resolved using cation-exchange chromatography (see Chapter 2), it was decided to attempt the resolution of a 2,3-dpp bridged complex, $[\{Ru(phen)_2\}_2(\mu\text{-2,3-dpp})]^{4+}$. Species with more flexible bridging moieties have proven notoriously difficult to resolve via our routine cation-exchange chromatographic procedures; effective column lengths in excess of thirty metres have failed to clearly resolve a mixture of the ΔΔ and ΛΛ isomers of 2,3-dpp bridged complexes. It was thought that such a complex would provide a significant test of the efficiency of this technique.

Initial attempts at the resolution of *rac*-$[\{Ru(phen)_2\}_2(\mu\text{-2,3-dpp})]^{4+}$ on a HiTrap column containing the bulge oligonucleotide were unsuccessful, although at an eluent concentration of 10 mM sodium phosphate buffer and 0.075 M sodium chloride significant elongation of the purple/pink complex band was observed. Consequently, the resolution was re-attempted with a *second* HiTrap column (this one containing the hairpin loop sequence) attached in serial to the first bulge column. Using an eluent of lower concentration (5 mM sodium phosphate buffer/0.0375 M sodium chloride) and a lower flow rate (*ca.* 0.1 mL min^{-1}) due to increased back-pressure, the elution proceeded quite slowly. However, the complex eventually resolved

into two purple-pink bands which eluted close together after 1.0-1.2 L of eluent had passed through the columns. While the bands were largely well-defined, they were not completely separated within the effective length of the column. Even so, CD spectra of the two bands again suggested that Band 1 and Band 2 were strongly enriched in the ΛΛ and ΔΔ enantiomers, respectively (see Figure 5.6). In contrast to the resolution of $[\{Ru(Me_2bpy)_2\}_2(\mu\text{-bpm})]^{4+}$, the elution order of the $[\{Ru(phen)_2\}_2(\mu\text{-2,3-dpp})]^{4+}$ enantiomers was representative of the relative binding affinities observed in FID assays (ΔΔ > ΛΛ with regards to binding affinity for both oligonucleotides). Upon addition to the bulge sequence, decreases of 70 and 49% were observed for samples partially-enriched in the ΔΔ and ΛΛ enantiomers, respectively; addition to the hairpin sequence yielded decreases of 73 and 59% for those same enantiomers (see Figure 5.3).

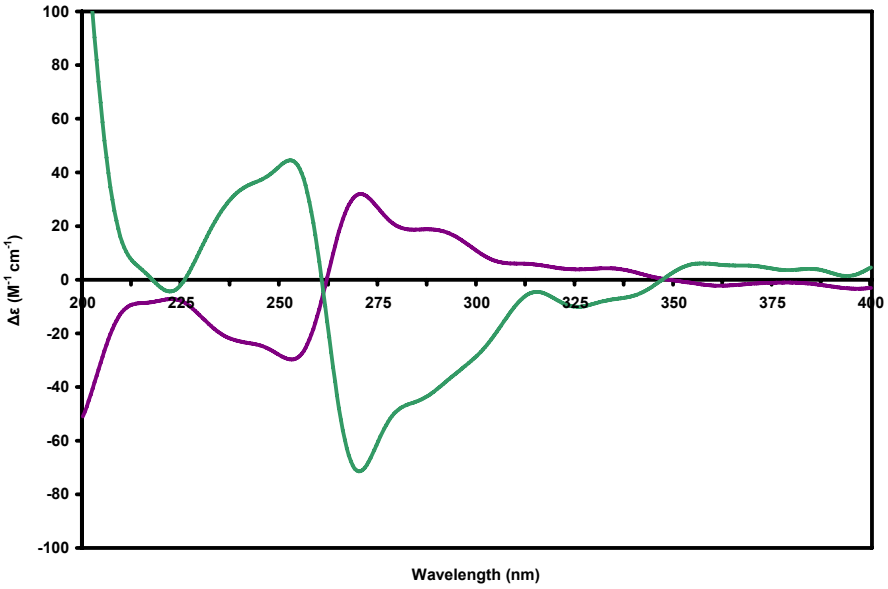

Figure 5.5
Near-resolution of recalcitrant enantiomers using non-duplex DNA. The CD spectra of the first (violet) and second (green) bands eluted from a mixture of ΔΔ- and ΛΛ-$[\{Ru(phen)_2\}_2(\mu\text{-2,3-dpp})]^{4+}$ separated on two HiTrap columns in serial, the first loaded with the bulge-containing oligonucleotide d(CCG**A**GAATTCCGG)$_2$, the second loaded with the hairpin-loop sequence d(CACTGGT**CTCTCT**ACCAGTG). The first band corresponds to the ΛΛ enantiomer, the second to the ΔΔ enantiomer.

The superior efficiency of these separations/resolutions compared to Sephadex-based chromatographic techniques can be attributed to a greater inherent selectivity in associations between metal complexes and immobilised DNA than in interactions with typical eluent anions.

Given the intrinsic chirality of nucleic acids, this selectivity may very well arise due to discrimination between different metal complexes, or the stereoisomers of those complexes, by the DNA itself. The commonly-observed preference of right-handed DNA to selectively bind to octahedral stereocentres of the Δ-configuration appears to extend to dinuclear species: resolutions of racemic mixtures of the ΔΔ and ΛΛ enantiomers generally make apparent a larger DNA-binding affinity in the former. However, it should be noted that the *meso* (ΔΛ) diastereoisomer, possessing a metal centre of each configuration, exhibits the greatest affinity in a number of species. This observation – confirmed through several other techniques (see preceding Chapters) – serves to highlight the importance of matching the overall geometry of the binding molecule to the contours of the binding site (DNA groove, bulge, loop, etc.), as well as the overall chiral association. Indeed, the particular interactions taking place between metal complex and DNA may encompass any of the numerous forces that contribute to the ill-defined mechanism of affinity chromatography: electrostatics, hydrophobicity, van der Walls contacts, chiral discrimination, and size-exclusion. Thus, efficient separations of non-enantiomeric species – diastereoisomers and different complexes – have also been accomplished and the procedure has the potential for effective separations of other non-chiral systems such as geometric isomers. Nevertheless, flexibility/conformational isomerism in the complexes being separated still presents a potentially complicating factor, albeit at a greatly-reduced extent comparative to the traditional ion-exchange techniques.

5.3.4 Scale-Up of the Technique

Given the success of the technique on small amounts of complex it was desirable to scale up the procedure to levels more comparable to the multi-milligram scale at which the cation-exchange chromatographic procedures are typically performed (i.e. preparative rather than analytical quantities). The scaled-up technique made use of the same medium contained within pre-packed HiTrap columns, albeit purchased in bulk and packed into a high-performance glass column of approximately 10-12 times the volume of the pre-packed version. While it was hoped that the larger dimensions of the column would facilitate the separation of up several milligrams of complex at a time, results indicate that the optimal amount of material that could be practically separated at a time was only 1-2 mg (*ca.* 1 μmol). This relatively disappointing capacity can be attributed to the fact that while the column is appreciably longer than its pre-

packed HiTrap counterpart, the *radius* of the scaled-up column is only slightly larger. As a result, the availability of surface binding sites during the loading of the scaled-up column is not significantly greater than that of the pre-packed column. The capacity of the column was overwhelmed by larger amounts of material, resulting in smearing of the analyte and inefficient separation of bands.

Nevertheless, the scaled-up technique was successful in reproducing the separations and resolutions of the HiTrap columns at a moderately larger scale. Adhering to plate theory, the increased length of the column yielded separations of greater resolution than the smaller counterpart; however, in some instances the exceptional efficiency of the technique complicated the separation. Complexes that completely separated/resolved in the first few centimetres of the column sometimes underwent significant diffusion as they passed down the rest of the length of the column. The result is a significant dilution of the product upon elution, potentially complicating characterisation by UV/Vis or CD spectroscopy. This phenomenon could be largely alleviated by increasing the concentration of the eluent upon clear separation of the mixed species (thus eluting the bands faster and with greater coherency), yet it remains a significant shortfall of the scaled-up technique. Overall, these observations imply that the ideal apparatus for these DNA affinity chromatography techniques is most likely a column of intermediate length between the HiTrap and scaled-up columns, but with a considerably larger radius.

5.3.5 $[Ru(phen)_3]^{2+}$ Sequence Selectivity

The archetypical DNA-binding polypyridylruthenium(II) complex $[Ru(phen)_3]^{2+}$ was employed to investigate the utility of the technique in resolving mononuclear species. Given that polysaccharide matrices have themselves demonstrated some resolving power,[51, 52] the complex was first passed down a Streptavidin Sepharose column that had yet to be loaded with DNA. Ultimately a single, somewhat elongated band eluted relatively quickly from the column; CD measurements performed on clippings taken from the front and back of this single band revealed some enantioenrichment (Δ eluting faster than Λ). This suggests that while the matrix itself possesses some minor resolving capabilities (attributable to the streptavidin protein and/or Sepharose polysaccharide), with a greater affinity for the Λ enantiomer, the complex possesses little affinity for the support alone.

Resolution of a racemic mixture of $[Ru(phen)_3]^{2+}$ on non-duplex oligonucleotides (the bulge and hairpin sequences) was likewise relatively inefficient, contrasting the outcomes observed for dinuclear species. The mixture eluted quite slowly with 5 mM sodium phosphate buffer/0.0375 M sodium chloride but could not be resolved into two distinct bands within the 2.5 cm length of a HiTrap column nor within the *ca.* 10 cm length of the scaled-up column. Nevertheless, significant elongation of the single band was observed, again suggesting that resolution was underway; CD measurements of the front and back of the band showed enrichment in the Δ and Λ bands, respectively, but to a larger degree than in the case where no DNA was present. Both non-duplex oligonucleotides seemed to be similarly inefficient in resolving the complex, implying relatively poor enantioselectivity between $[Ru(phen)_3]^{2+}$ and non-duplex sequences. It might be envisioned that the non-duplex features of the oligonucleotides (bulge site or hairpin loop) are too large to neatly accommodate the relatively small mononuclear species as they do the dinuclear complexes. Accordingly, the association between a mononuclear complex and oligonucleotide, and the enantioselectivity inherent in that association, must be attributed to interactions with *duplex* sections of the oligonucleotide. Given the relatively poor affinity of $[Ru(phen)_3]^{2+}$ for DNA in general, little distinction between enantiomers is actually observed; indeed, the selectivity that *is* observed actually contradicts the previously established preference of Δ-$[Ru(phen)_3]^{2+}$ for DNA.[34, 35] It is possible that the Δ > Λ enantioselectivity of the DNA is negligible compared to the Λ > Δ selectivity of the Streptavidin Sepharose matrix, and that the polyanionic DNA instead serves to enhance the electrostatic attraction between the complex and stationary phase, exacerbating the structural selectivity of the matrix.

The use of duplex DNA sequences proved to be much a more effective means of resolving *rac*-$[Ru(phen)_3]^{2+}$, at least in the case of the oligonucleotide $[d(AT)_6]_2$. A HiTrap column loaded with this oligonucleotide was able to resolve *rac*-$[Ru(phen)_3]^{2+}$ into two distinct bands – Δ (Band 1) and Λ (Band 2) {see Figure 5.7} – upon elution with 5 mM sodium phosphate/0.0375 M sodium chloride buffer solution. A mixed sequence oligonucleotide, $d(CCGGAATTCCGG)_2$ {the control (bulge free) version of the bulge sequence}, was unable to affect complete resolution of the racemic mixture, instead giving rise to a degree of enantioenrichment of similar magnitude to that obtained through the use of non-duplex DNA. Once again, the Λ enantiomer exhibited the greater affinity for the column, with Δ-$[Ru(phen)_3]^{2+}$ eluting first. The degree of enantioselectivity of the oligonucleotide can again be

related to the strength of the association between it and the complex. AT-rich sequences are well-known to be particularly favourable binding sites for metal complexes owing to the increased electronegative charge and narrower (yet more flexible) minor groove of such sites. Thus, the increased affinity of the complex for the AT sequence potentially heightens the selectivity of the Streptavidin Sepharose matrix, yielding a greater efficiency in the resolution of *rac*-$[Ru(phen)_3]^{2+}$ compared to the mixed-sequence of the bulge control oligonucleotide.

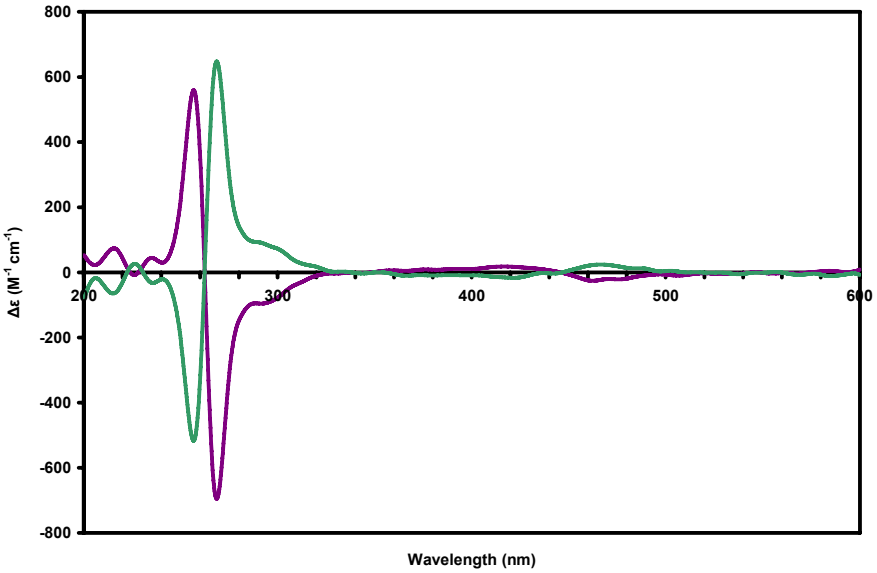

Figure 5.7
Resolution of $[Ru(phen)_3]^{2+}$ on $[d(AT)_6]_2$. The CD spectra of the first (violet) and second (green) $[Ru(phen)_3]^{2+}$ bands eluted from a HiTrap column loaded with an AT-rich duplex correspond to the Δ and Λ enantiomers, respectively.

5.3.6 $[Ru_2(qtpy)_3]^{4+}$ Sequence Selectivity

The affinity chromatography technique is presently being employed to resolve the supramolecular helicates being synthesised and studied by Mr. Christopher Glasson and Prof. George Meehan (JCU). Hannon and co-workers have reported the chiral resolution of similar helicates using cellulose columns,[40, 53] with DNA-binding studies on the pure enantiomers revealing a general affinity for the major groove.[54-57] Preliminary investigations into the efficacy of DNA-affinity chromatography in the resolution of helicates has revealed that the complex $[Ru_2(qtpy)_3]^{4+}$ (see Figure 5.8 for the structure) possesses an exceptional enantioselectivity for the $[d(AT)_6]_2$ sequence: the ΛΛ enantiomer (M {left-handed} helicate)

essentially elutes from the $[d(AT)_6]_2$-loaded column with the solvent front, whereas the ΔΔ enantiomer (P {right-handed} helicate) takes several hours to elute from the column. This resolution was also performed using columns loaded with the bulge-containing oligonucleotide $d(CCG\mathbf{A}GAAATTCCGG)_2$, the hairpin loop sequence d(CACTGGT**CTCTCT**ACCAGTG), and an all-GC sequence $d(CGCGCGCGCGCG)_2$; while in each instance there was still an impressive separation of enantiomers, none of these oligonucleotides were capable of replicating the degree of enantioselectivity observed when using the AT sequence. Further experiments intended to elucidate the selectivity of this complex and analogues featuring functionalised quaterpyridine ligands are currently being undertaken.

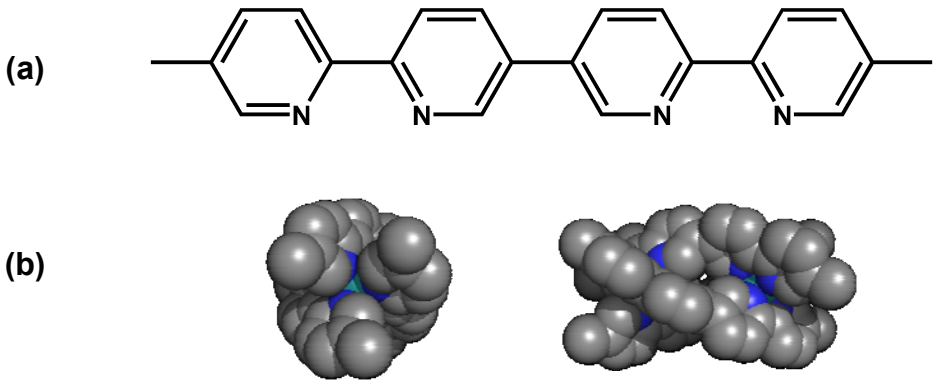

Figure 5.8
The supramolecular helicate $[Ru_2(qtpy)_3]^{4+}$. (a) The structure of 5,5‴-dimethyl-2,2′:5′,5″:2″,2‴-quaterpyridine (qtpy), and **(b)** two views of a model of ΔΔ-(P)-$[Ru_2(qtpy)_3]^{4+}$ (hydrogen atoms omitted for clarity).

5.3.7 Validating the DAPI-Displacement Fluorescence Assay

As discussed in Chapter 3, the ethidium bromide-based fluorescent intercalator displacement (FID) assay proved to be an effective high-throughput means of assaying the relative DNA-binding affinities and stereoselectivities of numerous metal complexes against multiple oligonucleotides. While the results of these surveys were predominantly in agreement with results obtained through other methods (notably NMR, equilibrium dialysis and affinity chromatography) a small number of inconsistencies *were* encountered. Modification of the FID assay to incorporate a minor groove-binding dye, DAPI, rather than the intercalator ethidium

bromide was found to rectify these discrepancies, yielding results that reflect the affinities implied by these other methods.[58]

Three specific cases, each of which presented suspect FID stereoselectivities when binding to a bulge-containing oligonucleotide {d(CCG**A**GAATTCCGG)$_2$}, were used to validate the DAPI-based assay. The first and most notable discrepancy involved FID results that suggested that the enantiomers of [{Ru(Me$_2$bpy)$_2$}$_2$(μ-bpm)]$^{4+}$ bound to the bulge-containing oligonucleotide with equal affinity. This was known to be erroneous as NMR experiments had previously demonstrated the total enantioselectivity of this complex with the same oligonucleotide.[48, 49] The greater affinity of the ΔΔ for the bulge sequence was reaffirmed in the affinity chromatography experiment described in §5.3.3. A second significant anomaly in the FID results pertained to the relative bulge-binding affinities of *meso*- and ΔΔ-[{Ru(phen)$_2$}$_2$(μ-dppm)]$^{4+}$ – the assay found no discernable difference between the two, whereas affinity chromatography experiments readily separated a mixture of the two diastereoisomers. The *meso* isomer eluted from the column before the ΔΔ enantiomer (as evidenced by the CD spectra of bands 1 and 2 – see Figure 5.9), suggested a greater bulge-binding affinity in the latter stereoisomer.

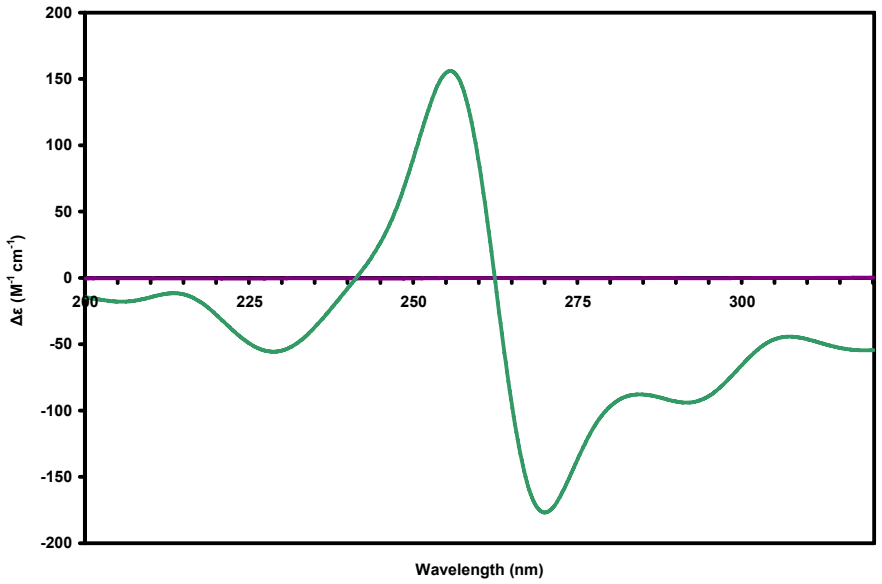

Figure 5.9
Separation of *meso* and ΔΔ-[{Ru(phen)$_2$}$_2$(μ-dppm)]$^{4+}$ on d(CCGAGAATTCCGG)$_2$. The CD spectra of the first (violet) and second (green) **[{Ru(phen)$_2$}$_2$(μ-dppm)]$^{4+}$** bands eluted from a HiTrap column loaded with a bulge-containing duplex correspond to the *meso* and ΔΔ enantiomers, respectively.

The third and final significant anomaly encountered within the FID assay involved the enantioselectivity of the association between the bulge sequence and the enantiomers of the flexible-bridged dinuclear species $[\{Ru(phen)_2\}_2(\mu\text{-bb7})]^{4+}$. FID results suggested that the ΛΛ enantiomer exhibited the higher binding affinity, whereas affinity chromatography indicated that exactly the opposite was true. Indeed, using the scaled-up affinity chromatography technique complete separation of the two enantiomers was achieved, whereas typical cation-exchange techniques were unable to resolve such a racemic mixture.[43] The identities of the eluted bands were confirmed by means of CD spectroscopy, with the ΛΛ form eluting first (see Figure 5.10). The preferential selectivity of the bulge sequence for the ΔΔ enantiomer was further confirmed in equilibrium dialysis experiments performed by Dr. Caitriona Spillane (JCU).[58] In each instance, repeating the fluorescent dye-displacement assay with DAPI instead of ethidium bromide resulted in fluorescence decreases that reflected the selectivities observed using DNA-affinity chromatography (refer to Chapter 3 for more details on the DAPI-displacement fluorescence assay). Thus, the validity of the DAPI-based technique was firmly established.

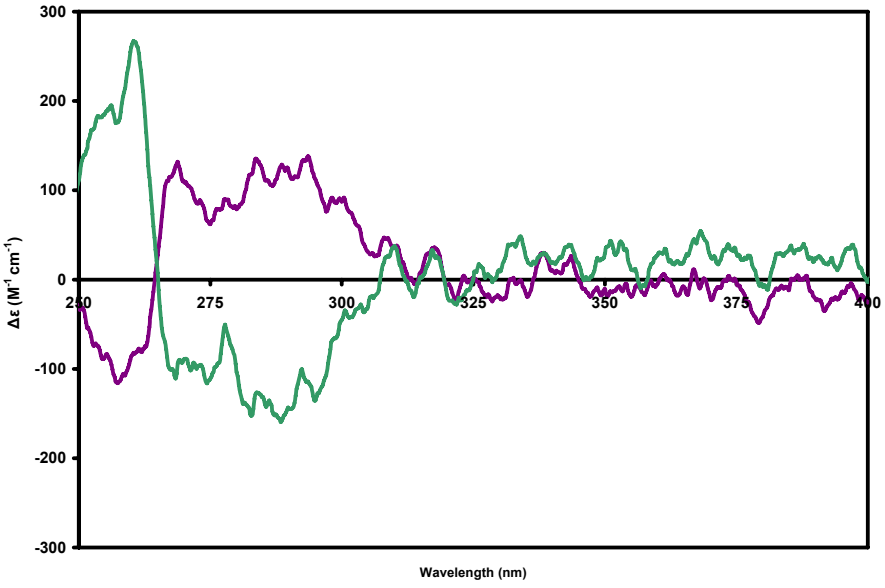

Figure 5.10
Resolution of $[\{Ru(phen)_2\}_2(\mu\text{-bb7})]^{4+}$ on d(CCGAGAATTCCGG)$_2$. The CD spectra of the first (pink) and second (green) **$[\{Ru(phen)_2\}_2(\mu\text{-bb7})]^{4+}$** bands eluted from a HiTrap column loaded with a bulge-containing duplex correspond to the ΛΛ and ΔΔ enantiomers, respectively. Spectra were recorded at high dilution, resulting in a poor signal-to-noise ratio.

5.3.8 Resusability of the Medium

The DNA-loaded Streptavidin Sepharose medium has proven highly reusable, maintaining its separating capabilities even after six months of storage (refrigerated in a 20% ethanol solution). Furthermore, the medium does not exhibit the tendency to discolour; after multiple uses the affinity support remained white, whereas under similar use the cation-exchange medium SP Sephadex would have become stained to the point of being unusable (dependent upon the complex(es) being chromatographed).

The DNA-affinity chromatography support also has the capability to be regenerated with a different oligonucleotide should alternative selectivities need to be investigated and/or exploited. While the interaction between the Sepharose-bound streptavidin and the biotinylated oligonucleotide maintains its stability under standard elution and storage conditions, an agent as simple as hot water (> 70 °C) is capable of breaking the streptavidin-bond without denaturing the streptavidin, thus ensuring its reusability.[59] This phenomenon was successfully demonstrated on a DNA-charged HiTrap column: hot water was continuously pumped through the column for 20 minutes with the eluate monitored spectrophotometrically for eluted DNA. The hot water wash did indeed eliminate a large amount of DNA, whereas subsequent cold water washes eluted no DNA. When the column had cooled back to room temperature and was re-equilibrated with buffer solution, an alternative oligonucleotide was successfully loaded onto the support ready for further chromatographic separations. Re-annealing and re-using the eluted biotinylated oligonucleotide at a later date remains an attractive albeit untested possibility.

5.4 CONCLUSIONS & FUTURE DIRECTIONS

As detailed above, DNA-affinity chromatography has proven itself as a highly-efficient means of separating stereoisomers of polypyridylruthenium(II) complexes. On the small scale the technique provides a robust means of establishing the relative binding affinities of metal complexes to a particular oligonucleotide. While the scaled-up technique did not fulfil our more optimistic expectations, it still offers the potential to readily isolate small amounts of a stereochemically-pure sample – sufficient for an NMR experiment, for example. Nevertheless, large scale preparative requirements currently remain best-handled by the cation-exchange chromatographic methods.

The DNA-affinity chromatography technique was found to be a valuable asset in confirming the inconsistencies in our original FID assays, thus facilitating the development of a more accurate DAPI-based modification of the assay. Future advances in the DNA-affinity methodology will most likely involve the establishment of a quantitative relationship between the retention times of complexes and their binding affinities for a given oligonucleotide. The assessment of binding affinity (be it relative or quantitative) using this methodology cannot be considered a high-throughput assay, however it does offer a considerable advantage over techniques such as the FID assay (and its DAPI-based derivative): the interactions being observed are a direct equilibrium competition between complexes (or isomers) for an oligonucleotide binding site, rather than a relatively ambiguous displacement mechanism. Such fluorescence-based assays provide an accurate means of surveying a library of metal complex/oligonucleotide interactions, but the complexities of the mechanism hinder the potential quantitative application of the technique. Even without a quantitative application, affinity chromatography asserts itself as a valuable intermediary procedure – between the broad surveys of fluorescence assays and the specificity of NMR investigations – for studying metal complex-oligonucleotide interactions.

In summary, the extraordinary efficiency and potential reusability of the DNA-affinity medium makes this chromatographic technique a highly-promising means of establishing the DNA-binding affinities of metal complexes. Currently, such analyses remain qualitative in nature, however a quantitative application of the technique remains a real possibility. Due to the cost of scaling up the DNA-affinity technique, traditional cation-exchange chromatographic techniques remain the best option for preparing large amounts of a stereochemically-pure complex.

5.5 REFERENCES

1. E. Hochuli, *Pure Appl. Chem.*, **1992**, *64*, 169-184.
2. P. Cuatrecasas and C. B. Anfinsen, *Annu. Rev. Biochem.*, **1971**, *40*, 259-278.
3. J. G. Dorsey, W. T. Cooper, B. A. Siles, J. P. Foley and H. G. Barth, *Anal. Chem.*, **1998**, *70*, 591R-644R.
4. W. Clarke and D. S. Hage, *Sep. Purif. Rev.*, **2003**, *32*, 19-60.
5. E. Frieden, *J. Chem. Ed.*, **1975**, *52*, 754-761.
6. K. Huse, H.-J. Böhme and G. H. Scholz, *J. Biochem. Biophys. Methods*, **2002**, *51*, 217-231.
7. V. I. Muronetz and T. Korpela, *J. Chromatogr. B*, **2003**, *790*, 53-66.
8. G. Mintz and L. Glaser, *Anal. Biochem.*, **1979**, *97*, 1979.
9. H. Kitagawa, H. Nakada, A. Kurosaka, N. Hiraiwa, Y. Numata, S. Fukui, I. Funakoshi, T. Kawasaki and I. Yamashina, *Biochemistry*, **1989**, *28*, 8891-8897.
10. L. G. Moore, W. Ng-Chie, S. Lun, S. B. Lawrence, W. Young and K. P. McNatty, *Gen. Comp. Endocrinol.*, **1997**, *106*, 30-38.
11. P. R. Manna, L. Joshi, V. N. Reinhold, M. L. Aubert, N. Suganuma, K. Pettersson and I. T. Huhtaniemi, *Hum. Mol. Genet.*, **2002**, *11*, 301-315.
12. P. Cuatrecasas, M. Wilchek and C. B. Anfinsen, *Biochemistry*, **1968**, 636-643.
13. V. I. Muronetz, M. Sholukh and T. Korpela, *J. Biochem. Biophys. Methods*, **2001**, *49*, 29-47.
14. G. Feinstein, *FEBS Lett.*, **1970**, *7*, 353-355.
15. Y.-C. Shi, Y.-M. Jiang, D.-X. Sui, Y.-L. Li, T. Chen, L. Ma and Z.-T. Ding, *J. Chromatogr. A*, **1996**, *742*, 107-112.
16. C. Tozzi, L. Anfossi and G. Giraudi, *J. Chromatogr. B*, **2003**, *797*, 289-304.
17. T. Makriyannis and Y. D. Clonis, *Biotechnol. Bioeng.*, **1997**, *53*, 49-57.
18. Y. D. Clonis, N. E. Labrou, V. P. Kotsira, C. Mazitsos, S. Melissis and G. Gogolas, *J. Chromatogr. A*, **2000**, *891*, 33-44.
19. H. Potuzak and P. D. G. Dean, *FEBS Lett.*, **1978**, *88*, 161-166.
20. H. Gadgil, S. A. Oak and H. W. Jarrett, *J. Biochem. Biophys. Methods*, **2001**, *49*, 607-624.
21. R. M. Litman, *J. Biol. Chem.*, **1968**, *243*, 6222-6233.
22. H. Gadgil, L. A. Jurado and H. W. Jarrett, *Anal. Biochem.*, **2001**, *290*, 147-178.
23. Y. D. Chung, H. C. Kwon, K. W. Chung, S. J. Kim, K. Kim and C. C. Lee, *Mol. Gen. Genet.*, **1996**, *251*, 347-351.
24. G. Schnapp, H.-P. Rodi, W. J. Rettig, A. Schapp and K. Damm, *Nucleic Acids Res.*, **1998**, *26*, 3311-3313.
25. H. Schaller, C. Nüsslein, F. J. Bonhoeffer, C. Kurz and I. Nietzschmann, *Eur. J. Biochem.*, **1972**, *26*, 474-481.
26. T. Y. Shih and M. A. Martin, *Biochemistry*, **1974**, *13*, 3411-3418.
27. P. Wils, V. Escriou, A. Warnery, F. Lacroix, D. Langneaux, M. Ollivier, J. Crouzet, J.-F. Mayaux and D. Scherman, *Gene Ther.*, **1997**, *4*, 323-330.
28. F. Mangani, G. Luck, C. Fraudeau and E. Vérette, *J. Chromatogr. A*, **1997**, *762*, 235-241.
29. J. Haginaka and J. Wakai, *Anal. Chem.*, **1990**, *62*, 997-1000.
30. D. Haupt, *J. Chromatogr. B*, **1996**, *685*, 299-305.

31. D. J. Jones, K. T. Nguyen, M. McLeish, D. P. Crankshaw and D. J. Morgan, *J. Chromatogr. B*, **1996**, *675*, 174-179.
32. C. Pham-Huy, B. Radenen, A. Sahui-Gnassi and J.-R. Claude, *J. Chromatogr. B*, **1995**, *665*, 125-132.
33. A. D. Baker, R. J. Morgan and T. C. Strekas, *J. Am. Chem. Soc.*, **1991**, *113*, 1411-1412.
34. J. K. Barton, A. T. Danishefsky and J. M. Goldberg, *J. Am. Chem. Soc.*, **1984**, *106*, 2172-2176.
35. C. Hiort, B. Nordén and A. Rodger, *J. Am. Chem. Soc.*, **1990**, *112*, 1971-1982.
36. M. Eriksson, M. Leijon, C. Hiort, B. Norden and A. Graslund, *Biochemistry*, **1994**, *33*, 5031-5040.
37. J. R. Aldrich-Wright, I. Greguric, R. S. Vagg, K. Vickery and P. A. Williams, *J. Chromatogr. A.*, **1995**, *718*, 436-443.
38. C. M. Shelton, K. E. Seaver, J. F. Wheeler and N. A. P. Kane-Maguire, *Inorg. Chem.*, **1997**, *36*, 1532-1533.
39. P. P. Pellegrini and J. R. Aldrich-Wright, *Dalton Trans.*, **2003**, 176-183.
40. M. J. Hannon, I. Meistermann, C. J. Isaac, C. Blomme, J. R. Aldrich-Wright and A. Rodger, *Chem. Commun.*, **2001**, 1078-1079.
41. B. J. Herbert, H. E. Carpenter, N. A. P. Kane-Maguire and J. F. Wheeler, *Anal. Chim. Acta*, **2004**, *514*, 27-35.
42. J. L. Morgan, D. P. Buck, A. G. Turley, J. G. Collins and F. R. Keene, *J. Biol. Inorg. Chem.*, **2006**, *11*, 824-834.
43. J. L. Morgan, C. B. Spillane, J. A. Smith, D. P. Buck, J. G. Collins and F. R. Keene, *Dalton Trans.*, **2007**, 4333-4342.
44. C. M. Eppler, J. D. Hulmes, J.-B. Wang, B. Johnson, M. Corbett, D. R. Luthin, G. R. Uhl and J. Linden, *J. Biol. Chem.*, **1993**, *268*, 26447-26451.
45. H. M. Alloush, J. L. López-Ribot, B. J. Masten and W. L. Chaffin, *Microbiology*, **1997**, *143*, 321-330.
46. S. L. Williams, M. E. Eccleston and N. K. H. Slater, *Biotechnol. Bioeng.*, **2005**, *89*, 783-787.
47. B. A. Katz, *J. Mol. Biol.*, **1997**, *274*, 776-800.
48. B. T. Patterson, J. G. Collins, F. M. Foley and F. R. Keene, *J. Chem. Soc., Dalton Trans.*, **2002**, 4343-4350.
49. J. A. Smith, J. G. Collins, B. T. Patterson and F. R. Keene, *Dalton Trans.*, **2004**, 1277-1283.
50. J. L. Morgan, D. P. Buck, A. G. Turley, J. G. Collins and F. R. Keene, *Inorg. Chim. Acta*, **2006**, *359*, 888-898.
51. N. C. Fletcher, P. C. Junk, D. A. Reitsma and F. R. Keene, *J. Chem. Soc., Dalton Trans.*, **1998**, 133-138.
52. T. J. Rutherford, P. A. Pellegrini, J. Aldrich-Wright, P. C. Junk and F. R. Keene, *Eur. J. Inorg. Chem.*, **1998**, 1677-1688.
53. I. Meistermann, V. Moreno, M. J. Prieto, E. Moldrheim, E. Sletten, S. Khalid, P. M. Rodger, J. C. Peberdy, C. J. Isaac, A. Rodger and M. J. Hannon, *Proc. Nat. Acad. Sci. USA*, **2002**, *99*, 5069-5074.
54. C. Uerpmann, J. Malina, M. Pascu, G. J. Clarkson, M. V., A. Rodger, A. Grandas and M. J. Hannon, *Chem. Eur. J.* , **2005**, *11*, 1750-1756.
55. G. I. Pascu, A. C. G. Hotze, C. Sanchez-Cano, B. M. Kariuki and M. J. Hannon, *Angew. Chem. Int. Ed.*, **2007**, *46*, 4374-4378.

56. E. Moldrheim, M. J. Hannon, I. Meistermann, A. Rodger and E. Sletten, *J. Biol. Inorg. Chem.*, **2002**, *7*, 770-780.
57. M. J. Hannon, V. Moreno, M. J. Prieto, E. Moldrheim, E. Sletten, I. Meistermann, C. J. Isaac, K. J. Sanders and A. Rodger, *Angew. Chem. Int. Ed.*, **2001**, *40*, 879-884.
58. C. B. Spillane, J. A. Smith, J. L. Morgan and F. R. Keene, *J. Biol. Inorg. Chem.*, **2007**, *12*, 819-824.
59. A. Holomberg, A. Blomstergren, O. Nord, M. Lukacs, J. Lundeberg and M. Uhlen, *Electrophoresis*, **2005**, *26*, 501-510.

Chapter 6

Epilogue

Ongoing studies into the nature of the interactions between small molecules and nucleic acids are not only essential to the design of more efficient and selective therapeutic and diagnostic agents but they also provide invaluable insights into the structural-functional relationships of these biomacromolecules. Progress in one of these aspects is reciprocated in the other: improved selectivity requires a greater understanding of which biologically-relevant features need to be targeted, and vice versa. To date, the selectivity of most utile nucleic acid-binding agents has been relatively modest, typically confined to short and/or relatively non-specific primary structural features (i.e. base sequences). With our growing knowledge of the importance of higher-order structures to many fundamental biological functions, the rational design of more efficacious agents demands a greater specificity that is inclusive of secondary structural features.

Owing largely to the success of cisplatin and its derivatives in treating cancer, transition metal complexes have been the subject of considerable attention with respect to their interactions with nucleic acids. Thus far, the majority of nucleic acid-binding complexes that have been adopted for therapeutic applications are covalently-binding species; however, the potential selectivity and utility of reversible, non-covalent interactions has received increased scrutiny in recent years. The basis of such studies has typically been polypyridyl complexes of d^6 metal centres {particularly Ru(II) and Rh(III)} which are often inherently inert, possess impressive photophysical, photochemical and redox properties, and have a well-defined synthetic chemistry. Furthermore, the six-coordinate, octahedral nature of such species gives rise to chiral complexes in the presence of two or three bidentate ligands; given the prevalence of homochirality in biological molecules there exists a promising potential to take advantage of complementary handedness in nucleic acid-metal complex interactions.

The bulk of studies into the nucleic acid-binding capabilities of metal complexes have concerned themselves with tris(bidentate) mononuclear species that interact by means of intercalation of one of their ligands between the base pairs of the target; however, mononuclear species are relatively limited in regards to their size and potential stereochemical variety, restricting their selectivity. Complexes of higher nuclearity offer not only an increased size by which to potentially recognise a longer target sequence, but the additional metal centres yield an enhanced electrostatic attraction and an increased stereochemical complexity which may be exploited in complementing a target site.

In light of this, the present studies have employed a variety of dinuclear polypyridylruthenium(II) minor groove-binding complexes in elucidating those factors that govern the affinity and selectivity of metal complex-nucleic acid interactions. A large variety of different complexes, incorporating a variety of bridging ligands ("linear", "angular" or "stepped-parallel" geometries) and terminal ligands (varying in aromaticity and hydrophobicity), were synthesised and the stereoisomers of each were separated using chromatographic techniques, as described in Chapter 2. FID surveys and electronic absorbance titrations, as discussed in Chapter 3, confirmed that the bulky nature of these complexes imbues them with a selectivity for more open secondary structures such as bulges and hairpin loops. The affinity of a complex for a given oligonucleotide was found to be governed by both the stereochemistry of the complex and the hydrophobicity of its terminal ligands. The former aspect embraces both the stereoisomerism of the complex (with the *meso* diastereoisomer typically exhibiting a greater affinity than either enantiomer) and the overall orientation of the terminal ligands of the complex, as governed by the geometry of the bridging ligand. Several of the more notable interactions were explored in NMR experiments, presented in Chapter 4, providing some insight into the specifics of these interactions between metal complexes and specific nucleic acid secondary structures. Included in these studies is the unexpectedly high-affinity association between a ppz-bridged complex and a *duplex*-only AT sequence, a particularly interesting interaction that was further studied using a biochemical assay.

The impressive selectivities demonstrated by many of these complexes for specific oligonucleotides (or features thereof) has lent itself to a reverse application of the metal complex-nucleic acid interaction in the form of affinity chromatography. As discussed in Chapter 5, DNA-based affinity chromatography columns can be used to separate complexes, diastereoisomers and enantiomers with exceptional efficiency. While on the scales used in these studies this technique is of most use to qualitative assessments of relative binding affinities, scaled-up techniques offer a highly effective, albeit expensive means to perform preparative separations. At present the technique is being used to investigate the exceptional enantioselectivity of series of supramolecular helicates.[1]

With the propensity of this class of rigid, dinuclear complex to target distinct secondary structural features now well-established, it remains for future studies to hone this selectivity to specific, biologically-significant non-duplex structures. Towards this end, a variety of different approaches will need to be undertaken (independently or jointly):

- *Flexible bridging ligands* – flexible bridges, such as the bb-type ligand employed by Kelly *et al*.[2] and Morgan *et al*.,[3] provide the means by which to allow a multi-nuclear complex to follow the groove of the target nucleic acid, with each metal centre binding at a favourable binding site. This offers a potentially higher affinity than complexes based upon the rigid bridging ligands of the present studies, the shape of which dictates interaction primarily via a single metal centre. Preliminary investigations involving dinuclear complexes based upon the afore-mentioned flexible ligands and oligonucleotides in which two potentially favourable binding sites are separated by an optimal distance show promising results in this regard.[4]

- *Oligonuclear complexes* – chain-like assemblies incorporating multiple metal centres (and associated functionalities) could conceivably be tuned so as to target several disparate binding sites simultaneously, greatly enhancing selectivity over species that interact via only one or two metal centres. Indeed, the synthetic route to larger multinuclear systems is well-established and routinely employed in studies of the electronic and spectroscopic properties of (polypyridyl) metal complex assemblies, but such systems have not yet been applied to nucleic acid-binding studies.

- *Mixed-mode binding* – complexes possessing multiple binding modes (intercalation *and* groove-binding, for instance) can offer enhanced selectivity and affinity over species which interact via a single mode as they exploit different the proclivities of disparate binding sites and the differing enthaplic and entropic considerations of each mode.[5]

- *Hydrogen-bonding* – hydrogen bonding functionality can be readily incorporated into terminal ligands of a nucleic acid-binding complex, affording some degree of sequence selectivity to the complex. One might envision a bulky complex that binds favourably to a specific bulge site as governed by appropriate sequence-matching hydrogen-bonding patterns on the peripheral ligands. The tuning of hydrogen-bonding functionality in a metal complex to match a specific base sequence has been demonstrated in the intercalating mononuclear rhodium complex Δ-α-[Rh{(R,R)-Me_2trien}(phi)]$^{3+}$ by Barton and co-workers.[6]

Thus, there remain many avenues to pursue in the design and study of nucleic acid-binding metal complexes; however, one aspect that must not be overlooked if such complexes are to have potential *in vivo* applications is that of cellular transport – do the complexes exhibit activity in the cell? A number of studies involving mononuclear complexes – intercalating and groove-binding – have demonstrated levels of cytotoxicity comparable with, if not better than, cisplatin.[7, 8] Aside from one recent study,[9] there has been little research into the cellular activity of dinuclear species. While cytotoxicity does not necessarily imply strong nucleic acid binding, it does confirm cellular uptake of the complexes (a property that has been related to the lipophilicity of the complex rather than its size or charge).[10] Indeed, cytotoxicity need not be the ultimate goal of nucleic acid-binding molecules, instead the complexes might be employed as a means of regulating gene expression through reversible interactions or as spectroscopic probes of specific structures or sequences *in vivo*.

Ultimately, the genre of metal complex utilised in the present studies represents a promising basis for the rational design of more efficacious drugs and probes, particularly those targeted at specific secondary structural features. By exploiting the well-established synthetic chemistry of polypyridylruthenium(II) complexes it should be possible to tune the selectivity of the complexes so as to attain high levels of specificity, thereby reducing the unpleasant side-effects that hamper present limited-specificity chemotherapeutics. In the interim, the process of ascertaining those structural features to which the complexes should be targeted will itself benefit from studies utilising non-duplex specific probes.

REFERENCES

1. C. R. Glasson, J. A. Smith, F. R. Keene and G. V. Meehan, **2007**, *unpublished work*.
2. F. M. O'Reilly and J. M. Kelly, *New J. Chem.*, **1998**, *22*, 215-217.
3. J. L. Morgan, C. B. Spillane, J. A. Smith, D. P. Buck, J. G. Collins and F. R. Keene, *Dalton Trans.*, **2007**, 4333-4342.
4. J. A. Paul, M. J. Pisani, D. P. Buck, J. G. Collins and F. R. Keene, **2007**, *unpublished work*.
5. J. B. Chaires, *Biopolymers*, **1997**, *44*, 201-215.
6. B. P. Hudson, C. M. Dupureur and J. K. Barton, *J. Am. Chem. Soc.*, **1995**, *117*, 9379-9380.
7. D.-L. Ma, C.-M. Che, F.-M. Siu, M. Yang and K.-Y. Wong, *Inorg. Chem.*, **2007**, *46*, 740-749.
8. C. B. Spillane, N. C. Fletcher, S. M. Rountree, H. van den Berg, S. Chanduloy, J. L. Morgan and F. R. Keene, *J. Biol. Inorg. Chem.*, **2007**, *12*, 797-807.
9. U. McDonnell, J. M. C. A. Kerchoffs, R. P. M. Castineiras, M. R. Hicks, A. C. G. Hotze, M. J. Hannon and A. Rodger, *Dalton Trans.*, **2008**, DOI: 10.1039/b711080d.
10. C. A. Puckett and J. K. Barton, *J. Am. Chem. Soc.*, **2007**, *129*, 46-47.